Nanoparticles for Biomedical Applications: Photothermal Therapy and Nuclear Delivery

by

Taeyjuana Y. Curry

A dissertation submitted in partial fulfillment
of the requirements for the degree of
Doctor of Philosophy
(Physics)
in The University of Michigan
2013

Doctoral Committee:

Professor Raoul Kopelman, Chair
Professor Theodore Goodson
Professor Jens-Christian Meiners
Professor Bradford Orr
Professor Martin Philbert

DEDICATION

Quiltonya Grant

King & Merie Cooper

Kenta Mobley

Eloise Williams

ACKNOWLEDGEMENTS

"If I have seen further it is by standing on ye shoulders of Giants."
~Sir Isaac Newton

I've wanted to be a teacher for as long as I can remember. My love for learning most likely comes from that desire as it became quite clear early on that to be an effective teacher, I had to first be a committed student. I am most appreciative of the many exemplary educators under whose tutelage my desire for knowledge and intrigue with education was constantly affirmed and nurtured. I would like to acknowledge a small fraction of my former instructors and counselors who have contributed to my success in no small way. My first grade teacher, Mrs. Erwin, identified my mischievous behavior as the result of boredom/lack of engagement. She had me tested for gifted/talented classes rather than writing me off as a problem child. The next year, my 2nd grade teacher, and gifted/talented teacher for grades 3rd-5th, Mrs. Ham helped me discover my love of mathematics and the sciences and instilled a belief in me that anything was possible despite what others sometimes perceived as my limitations. In 7th grade, Mrs. Chamberlain, my guidance counselor saw great potential in me and helped me to obtain my first scholarship for college. Finally, in high school, Dr. Steele taught me that once I set a personal goal, it is imperative that I never lose sight of or give up on that goal it until I have

accomplished it. Mr. Shaw and all of the staff of the USF Project Upward Bound program helped me to focus on becoming the most well rounded candidate before applying for college. Dr. Patricia Stith and the FSU FGAMP program introduced me to the reality of graduate education and provided me with the information and opportunities for undergraduate research that were necessary to obtain admission in to the prestigious University of Michigan. All of these lessons and personal contributions certainly propelled me toward my ultimate goal of obtaining a PhD.

I sincerely thank my adviser, Dr. Raoul Kopelman, for taking me on as his graduate student, helping to secure funding, and providing the opportunity to fulfill one of my life's goals. I also thank all of my committee members for their time, effort, constructive criticisms and thoughtful feedback that helped to shape my dissertation. The departments of Physics, Chemistry, and Biophysics have also supported me throughout my graduate education. I am grateful to all of the Kopelman group members who I've had the privilege of working with during my time in the lab. I am especially thankful for Drs. Epstein and Si whose guidance, mentorship, and friendship have certainly helped to shape me as a graduate student. I am very grateful for my formal and informal mentors, Drs. August Evrard, Daphne Watkins-Jacobs, Alec Galimore, and Deborah Mitchell. I'd like to acknowledge Rackham Graduate School, the Physics Department, AGEP, CEW and WISE for providing funding throughout my program.

My family and friends has also played such a pivotal role in my success. First and foremost, I must acknowledge my mother who for the better part of my

life has been my inspiration and pillar of strength. She, along with my grandfather, and aunt begin fostering what I'm told was a keen curiosity and thirst for learning even as a toddler. My siblings, Chyijuan, Chyijuana, Kimberly and Hewitt have always been a unique source of motivation for me, as I know they to me to set the standard. My older brother, Kentae, continues to inspire me though he is no longer with us. My dearest friends, Tai Ishia, Brandi, Amelia, and Juana have always supported me and believed in me even when my own belief faltered. My very best friend and significant other, Robert, has been undoubtedly the most crucial part of my support system in the last two and a half years. I owe so much of my completion of this program to his generosity, consideration, and love.

I also owe a debt of gratitude to following groups of people who have played crucial roles in my support system throughout the last six years. My closest sorority sisters, Oneshia, Shante', Sophia, Jackie, Jennifer, Natalie, Earnee, & Jamie for their love, support, and friendship that has surpassed our sorority ties. My "Michigan Family," April, Natalie, Ced, Brad, Kevin & Korey helped me to make Michigan my home away from home in initial years at the University of Michigan. My "Physics Family," Yisa, Mitaire, Ibrahima, Kim, Chuck, Ramon, Dennis, Anette, Genni, Renee', Laura, Leslie, Kim, Erica, Afi, Charity, Clarissa, and Nicole were all always willing to share their experiences and endowed me with an amazing Physics network. My Bethel AME family, especially Pastor Cousin, Reverend Whiten, and members of the Campus Outreach Ministry provided a strong spiritual network. My counselor, Brittany Bouffard of CAPS helped me to maintain some sense of sanity in the last 12

months of my program. Lastly, the dear friends I've garnered during my graduate school tenure, Kyla, Angie, Ebone', Will, and Monisha have truly become a part of my heart.

My deepest gratitude is to my Lord and Savior, Jesus Christ. I believe that He gave me a promise back in middle school that He would empower me to fulfill this dream. Although the journey has in now way be easy, He has never left me and it was through His grace and mercy that I finally finished. Amen.

TABLE OF CONTENTS

DEDICATION ..... **ii**

ACKNOWLEDGEMENTS ..... **iii**

LIST OF FIGURES ..... **xi**

ABSTRACT ..... **xvii**

Chapter 1 Introduction **1**

1.1 Motivation & Background **1**

1.1.1 Nanoparticle-mediated Sensing 2

1.1.2 Nanoparticle-Mediated Imaging 5

1.1.3 Nanoparticle-Mediated Therapy 7

1.2 Overview of This Dissertation **11**

1.3 Figures **16**

1.4 References **17**

Chapter 2 Photothermal Therapy of Cancer Cells Mediated by Blue Hydrogel Nanoparticles **27**

2.1 Introduction **27**

2.1.1 Background 30

2.2 Materials and Methods **32**

2.2.1 Materials 32

2.2.2 Light Source 33
2.2.3 Cell Culture 33
2.2.4 Nanoparticle Synthesis & Characterization 33
2.2.5 Cellular Uptake Assay 40
2.2.6 Photothermal Therapy & Live/Dead Assay 41
2.2.7 Controls 42
2.3 Results & Discussion 42
2.3.1 Cytotoxicity 42
2.3.2 Cellular Uptake 44
2.3.3 Photothermal Therapy 44
2.4 Conclusions 46
2.5 Acknowledgments 47
2.6 Figures 48
2.7 References 59
Chapter 3 Surface Optimization of Gold Nanoparticles for Controlled Delivery into Cancer Cell Nuclei 63
3.1 Introduction 63
3.2 Background 66
3.3 Materials & Methods 68
3.3.1 Materials 68
3.3.2 Cell Culture 68
3.3.3 Nanoparticle Fabrication 69
3.3.4 Nanoparticle Surface Modification 70

3.3.5 Concentration Study 71
3.3.6 Optimization of Surface Modifications 71
3.4 Results and Discussion 73
3.4.1 Concentration Study 73
3.4.2 PEG 5K Optimization 74
3.4.3 $(RGD)_4$ Optimization 75
3.4.4 Incubation time 76
3.4.5 Confirmation of Nuclear Delivery 77
3.5 Conclusions 78
3.6 Acknowledgements 79
3.7 Figures 80
3.8 References: 89
Chapter 4 Optimization of Photothermal Therapy of Cancer Cells via Nuclear Delivery of Surface Modified Au Nanoparitcles 95
4.1 Introduction 95
4.2 Theoretical background 97
4.3 Materials & Methods 100
4.3.1 Materials 100
4.3.2 Cell culture 101
4.3.3 Nanoparticle Characterization & Surface Modification 101
4.3.4 Imaging/Live-dead Assay 102
4.3.5 Photothermal Therapy (PTT) 103
4.3.6 Controls 104

4.3.7 Transmission Electron Microscopy 105

4.4 Results & Discussion 105

4.4.1 Short-term studies 106

4.4.2 Long-term studies 108

4.4.3 Intracellular Nanoparticle Fate 108

4.5 Conclusions 110

4.6 Acknowledgements 111

4.7 Figures 112

4.8 References 123

Chapter 5 Conclusions & Future Directions 126

5.1 Conclusions 126

5.2 Future Directions 129

5.2.1 Clinical Use of CB-PAA Nanoparticles 129

5.2.2 Faster Nuclear Delivery of Surfaced Modified Gold Nanoparticles ... 131

5.2.3 Strategies for Improving Gold Nanoparticle-Mediated Photothermal Therapy 132

5.3 References 134

LIST OF FIGURES

Figure 1.1: Schematics PEBBLE sensors [Lee *et al*. Imaging and Spectroscopic Analysis of Living Cells: Optical and Spectroscopic Techniques, **2012**]: (A) Single core NP loaded with both sensing and reference components), (B) Core–shell PEBBLE (core–shell NPs with spatially separated sensing and reference components), (C) Temperature-sensitive NP PEBBLE (NP matrix as a sensing unit). PEBBLE-mediated studies, (D) Intracellular Ca^{2+}[Si, *et al*. Analytical Chemistry*,* **2012**] and (E) oxygen sensing [Lee *et al.* Analytical Chemistry*,* **2012**]. 15

Figure 2.1: Size and zeta potential characterization of the CB-PAA NP was carried out using a Delsa Nano DLS particle sizer. CB-PAA NP are 80-95nm in diameter and have a zeta potential of 25-27mV.....42

Figure 2.2: Photobleaching of various concentrations of CB-PAA nanoparticle solutions. The degree of photobleaching was quantified as the percent difference in absorbance at 600nm before and after illumination. Error bars denote standard error, n=2.....43

Figure 2.3: Absorbance spectra of the filtrate of varying concentrations of CB-PAA NP solutions *after* 40 minutes illumination. The absorbance spectrum of 0.1mg/mL of CB-PAA NPs is also displayed for reference.....44

Figure 2.4: Top-Fluorescence spectra of ADPA in a mixed solution of CB-PAA NPs (0.6 mg/mL) at various time points; inset-close up view of 405nm peak used for calculations. Bottom-Linear fitted graph of fluorescence change with increasing irradiation times up to five minutes.....45

Figure 2.5: Temperature change for CB-PAA NP dissolved in DPBS at concentrations of 0.1, 0.6, and 1.2mg/mL. Initial starting temperature of the solutions was approximately 37° C.....46

Figure 2.6: Absorbance of CB-PAA NP dissolved in DPBS at concentrations between 0.1-0.35mg/mL; inset: graph of CB-PAA NP concentration versus peak absorbance value at 600nm used to calculate the concentration of filtered CB-PAA NP.....47

Figure 2.7: Fluorescent images of cells that had been previously incubated with CB-PAA NP and then exposed to PTT. The images were taken before, right after, and every 30 minutes post treatment. Green fluorescence indicates viable cells while red indicated dead cells.....48

Figure 2.8: Cell viability of HeLa cells after 24 hours incubation with increasing concentrations of CB-PAA nanoparticle solutions as determined by MTT assay. The results indicate no significant change in toxicity with increasing nanoparticle concentration. Error bars represent standard error in absorbance at 550nm. Note: No illumination.....49

Figure 2.9: CB-PAA NP uptake into cells after 24 hours of incubation analyzed by nanoparticle absorbance at 600nm. Error bars denote standard error (n=2). 50

Figure 2.10: Survival rates over time of the cells over a period of 3 hours after 20 minutes of PTT with CB-PAA NP solution concentrations of 0.2-1.2mg/mL. Error bars denote standard error in average number of live cells per time point; experiments were done in triplicates, except for 0.8mg/mL, which was done in duplicate. Note: Shaded area is illumination time.....51

Figure 2.11: Survival rates over time of cells treated with 0.6 mg/mL of CB-PAA in growth media for 24 hours with 10, 20, and 40 minutes of illumination time (PTT), and the control measurement (BLANK PAA NP, 40 minutes illumination time). Error bars represent the standard error in the average number of live cells at each time point; experiments were done in triplicates. All illuminations started at time 0.....52

Figure 3.1: Schematic diagram of targeted delivery of multi-targeted, biocompatible Au NPs into cell nucleus. The function of PEG is to maintain stability of Au NPs in media and prohibit non-specific binding to cells. RGD enables binding of the Au NPs to receptors on the cell membrane and induces intracellular delivery via endocytosis. NLS enables binding of the Au NPs to importin, which mediates nuclear transport.....70

Figure 3.2: (A) Representative UV-VIS absorption spectrum of colloidal gold nanoparticles prepared by femtosecond laser ablation and a transmission electron microscopy (TEM) picture of these colloidal gold nanoparticles is shown in the inset [Qian, *et al.* Journal of Physical Chemistry C, **2011**]. (B) Schematic of the sequential conjugation methods utilized to modify the surfaces of the nanoparticles.....71

Figure 3.3: Experimental determination of the amount of thiolated PEG 5K required to form a complete monolayer on the surface of the femtosecond laser generated gold nanoparticle. Size increase of the nanoparticle as increasing concentrations of PEG 5K was added to the surface was determined using Dynamic Light scattering. The increase in nanoparticle size as compared to unmodified gold nanoparticles is shown here.....72

Figure 3.4: Bright field images of cancer cells that were incubated for 24 hours with varying concentrations of gold nanoparticles surface modified with molar ratios of 150 PEG 5K & 1000 RGD per nanoparticle.....73

Figure 3.5: Bright field images of cancer cells. (3A) Cells that were incubated with surface modified gold NPs with varying molar ratios of PEG 5K per nanoparticle. (3B) Cells that were incubated with surface modified gold NPs with a molar ratio of 200 PEG 5K per nanoparticle and varying molar ratios of $(RGD)_4$ per nanoparticle. (3C) Cells that were incubated for varying times with gold nanoparticles that were sequentially conjugated with molar ratios of 200, 400, & 800 Of PEG 5K, $(RGD)_4$, and NLS, respectively.....74-75

Figure 3.6: TEM Confirmation of nuclear delivery. (A) Surface modified gold nanoparticles inside of the cell's nucleus are denoted by red circles. Gold nanoparticles located in the cytosol (circled in green) and within the lysosome/endosome complex (circled in blue) are also noted. (B) Zoomed out view of the same cancer cell. (C) Bright field image of cells before they were fixed.....76-77

Figure 4.1: (Top) TEM image and (Bottom) dynamic light scattering data (DLS) of unmodified gold nanoparticles. Average diameter of the nanoparticles is 30nm.....98

Figure 4.2: Temperature change of gold nanoparticles dissolved in cell media and illuminated continuously for 40 minutes. Starting temperature was in the biological range. Cell media was also illuminated as a control.....99

Figure 4.3: Representative images and composite image of Live/Dead assay utilized to characterized the efficacy of treatment. Top left: calcein channel (em. 510-520nm), top right: propidium iodide channel (em. 612-622), bottom left: DIC image, bottom right: composite image.....100

Figure 4.4: Viability of cells incubated with varying concentrations of gold nanoparticles modified with either PEG 5K, $(RGD)_4$ only or PEG 5K, $(RGD)_4$ with and NLS and then illuminated at 514nm for 30 minutes. All experiments were done in duplicates. Error bars denote standard error in the percent of live cells at a given time point. Representative images and composite image of Live/Dead assay utilized to characterized the efficacy of treatment. Top left: calcein channel (em. 510-520nm), top right: propidium iodide channel (em. 612-622), bottom left: DIC image, bottom right: composite image.....101-102

Figure 4.5: Viability of cells incubated with varying concentrations of gold nanoparticles modified with either PEG 5K, $(RGD)_4$ only or PEG 5K, $(RGD)_4$ with and NLS and then illuminated at 514nm for 30 minutes. All experiments were done in triplicates. Error bars denote standard error in the percent of live cells at a given time point.....103-104

Figure 4.6: Viability of cells incubated with varying concentrations of gold nanoparticles modified with either: TOP: PEG 5K, $(RGD)_4$ only or BOTTOM: PEG 5K, $(RGD)_4$ with and NLS and then illuminated at 514nm for 30 minutes. All experiments were done in triplicates. Error bars denote standard error in the percent of live cells at a given time point.....105

Figure 4.7: TEM confirmation of nuclear delivery in cells that were incubated with 500pM of gold nanoparticles modified with PEG 5K, $(RGD)_4$ and NLS peptides. LEFT: 5700X magnification, RIGHT: 13500 X magnification of the nucleus of the same cell. Appropriate scale bars are below each image.....106

Figure 4.8: TEM confirmation of nuclear delivery in cells that were incubated with 1nM of gold nanoparticles modified with PEG 5K, $(RGD)_4$ and NLS peptides. LEFT: 5700X magnification, RIGHT: 13500 X magnification of the nucleus of the same cell. Appropriate scale bars are below each image.....107

Figure 4.9: Comparison of the fate of gold nanoparticles once they are taken up by the cancer cell for TOP: 500pM and BOTTOM: 1nM nanoparticle concentrations. TEM images on the left are 5700X magnification and TEM images on the right are 13500X magnification of the same cells. Appropriate scale bars are below each image.....108

ABSTRACT

Nanoparticles for Biomedical Applications: Photothermal Therapy and Nuclear Delivery

by

Taeyjuana Y. Curry

Chair: Raoul Kopelman

Cancer is still a grand challenge faced by society today. Nanomedicine addresses many of the serious issues associated with conventional treatments. Nanoparticles (NPs) are advantageous for therapy because they are minimally invasive, have tunable characteristics and can be used as targeted and multifunctional treatment platforms.

This thesis focuses on the use of both polymeric and gold NPs for photothermal therapy (PTT) of cancer cells, and describes the surface engineering of gold NPs for optimized, cell specific nuclear delivery. The first ever use of the FDA approved Coomassie Brilliant blue (CB) dye as a photosensitizer for PTT of cancer is detailed. The CB dye is covalently linked into the matrix of biologically compatible, hydrogel NPs. Also, a portable, inexpensive, low intensity LED is used as the light source. Incubation with moderate NP concentrations, combined with relatively low light levels, yielded nearly complete cell death within 3 hours of treatment.

Another part of this dissertation research describes the stepwise surface engineering of specialty gold NPs for optimized delivery to cancer cell nuclei. These femtosecond laser ablation generated gold NPs have *virgin* surfaces to which cell-specific and nucleus-specific targeting peptides are directly attached. Efficient nuclear delivery was achieved using as little as 100pM of NPs solution, a concentration that is *at least* an order of magnitude lower than what has been previously reported in nuclear delivery studies involving gold NPs.

The aforementioned nuclear-targeted gold NPs were also successfully utilized for PTT of cancer cells *in vitro*. A drastic difference in treatment efficacy was observed when the therapy was mediated by gold NPs delivered into the nucleus compared to when the NPs remained outside the nucleus. In the former case, the cell viability drops dramatically at early times and complete cell death is observed at six hours post-treatment. In the latter case, the viability decreases slowly over time and a maximum change of approximately 50% is observed 12 hours post-treatment.

Overall this thesis provides several contributions to the field of Nanobiotechnology, through the presentation of highly effective, nanoparticle-mediated PTT. The latter can be easily incorporated into a multimodal approach for the treatment of cancer.

Chapter 1 Introduction

1.1 Motivation & Background

In the last decade, nanoparticles have emerged as effective platforms for diagnostics, imaging, sensing, and therapeutic studies in numerous fields of research. This emergence has facilitated major research breakthroughs including cancer diagnosis and treatment[1,2], early detection of chronic and debilitating diseases[3,4], rapid detection of bacteria growth for evaluation of antibiotic effectiveness[5,6], imaging enhancement, and intracellular sensing [7,8].

The increase and sustained growth in nanoparticle research primarily resides in its many advantages over more conventional techniques, which include the ability for non-invasive, quantitative and qualitative measurements of many physical and chemical intracellular processes. These measurements are usually achieved through facile incorporation of various molecular sensing agents into the nanoparticle platform, as well as surface modifications. Furthermore, nanoparticles provide an avenue through which a concentrated amount of sensing, diagnostic, or therapeutic agent, or a combination of two or more of these, can be delivered to target cells. This is more advantageous than other

methods of intravenous administration of dyes and drugs in which only low local concentrations are usually achieved due to the global spreading of the dose.

Another advantage associated with nanoparticles is the tunability of their size, shape, absorption, and surface characteristics. Nanoparticles sizes range from a few nanometers to hundreds of nanometers, and the currently employed shapes are variable and usually dictated by the nature of their purpose. Usually, the size and shape of the nanoparticles are easily adjusted during fabrication, using wet lab techniques. Nanoparticles can be shaped like spheres, stars, rods, pyramids, barbells, cylinders, etc., and can also be solid or hollow ("nanobottles"). Additionally, nanoparticle matrices greatly vary, depending on the intended purpose and the nature of the study; their structure can range from being metallic, polymeric, ceramic, carbon, or a hybrid thereof. Nanoparticle-mediated sensing, imaging, and therapy are three of the primary ways in which nanoparticles are currently being successfully used in academic research, and for clinical and industrial applications; however, this introductory chapter will focus on academic studies.

1.1.1 Nanoparticle-mediated Sensing

The ability to measure chemical and physical processes within a live cell in real time enables early detection of diseased cells, evaluation of a previously applied treatment, and the ability to monitor internal responses to changes in the cell environment, among other things. In particular, intracellular ion sensing is of substantial interest because of the important role ions play in maintaining healthy

physiological conditions within the cell. To this end, various molecular probes have been identified or fabricated for intracellular ion sensing; however, initial research studies involving these probes were plagued by many drawbacks, including nonspecific binding within the cells which led to reduced sensing capabilities, sequestration in cell compartments devoid of the ion of interest, interaction with other cell processes, and measureable toxicity. Nanoparticle-mediated intracellular sensing offers many advantages over other conventional forms of intracellular sensing, such as patch clamps and micro-optodes and electrodes. These advantages include being noninvasive, providing a biologically inert barrier between the sample and the sensor, enabling real time measurements, and facilitating sensing capabilities of multiple analytes in parallel.

The Kopelman group has a long-standing history sensing research, involving ions, molecules and radicals, by the use of so-called "PEBBLEs," an acronym for **P**hotonic **E**xplorers for **B**ioanalysis in **B**iologically **L**ocalized **E**mbedding; a schematic of some of the most commonly utilized PEBBLE schemes is shown in Figure 1.1A-1.1C. The PEBBLEs were fabricated using various nanoparticle matrices, including cross-linked polyacrylaminde, organically modified silane, cross-linked poly(decylmethacrylate), ormosil and sol-gel silica, and have been utilized for intracellular sensing of many ions, molecules and radicals, including H^+, Ca^{2+}, K^+, O_2, Zn^{2+}, Cl^-, Na^+, Mg^{2+}, Cu^{2+}, as well as O_2, H_2O_2, glucose and NO, OH, etc. [8-16]. The general premise guiding these studies involves the incorporation and/or encapsulation of, among others, ion sensitive

dyes within the nanoparticle matrix, thereby addressing many of the above mentioned drawbacks associated with simply staining the cells with “naked” molecular probes. For example, in a recent study conducted by Di Si, et al. [8], a rhodamine-based Ca^{2+} dye was loaded into the interior of nanoPEBBLEs, with a reference dye, Hilyte Fluor 647, conjugated to the nanoparticle matrix, shown in Figure 1.1D. The study demonstrated that this type of nanoparticle construction avoids many of the issues commonly associated with intracellular Ca^{2+} sensing. The study also illustrated reliable, ratiometric intracellular measurements, a lack of nonspecific binding of the sensing dye to intracellular proteins, or dye leaching, and avoiding subsequent sequestration into organelles. Furthermore, the incorporation of the sensing dye into the nanoparticle matrix enabled a high certainty that the calibration completed in solution *in vitro,* prior to treating the cells, remained accurate once the nanoPEBBLEs were inside of the cells.[8] Another notable study conducted within the Kopelman group involved the successful fabrication of 30nm targeted oxygen sensors for intracellular use [17], shown in Figure 1E. As in the previous studies, the nanosized PEBBLE matrix was made of a polyacrylamide hydrogel, however, in this study the nanoparticles were attached with either TAT-Cys, a cell penetrating peptide, or the F3-Cys peptide, which facilitates preferential uptake into cancer cells. One important aspect of these sensors was the incorporation of both a sensing dye, G2, and a reference dye, Alexa 647 dextran 10,000, or HiLyte 680 SE, which emits in the near infrared range (NIR), and thereby increases the tissue penetration depth, due to low light absorption and scattering at the NIR region, and also improves

the signal to noise ratio due to reduced autofluorescence and photobleaching; thus addressing some of the challenges commonly associated with imaging and sensing schemes in tissues. [17]

1.1.2 Nanoparticle-Mediated Imaging

Oftentimes, the first steps of diagnosing a disease or disorder involve imaging of the tissue or region of interest. Imaging modes, including X-ray, MRI, and ultrasound are routinely used for such purposes; however, these imaging modalities are limited in that they cannot provide information on cellular and molecular level activity. Furthermore, these imaging techniques are normally used after the disease or disorder has already presented itself clinically and has begun to affect the patient's quality of life. These shortcomings, along with others not detailed here, have opened the door for the development of imaging techniques that provide real-time cellular information, i.e. direct visualization of biological processes within cells and tissues. Nanoparticle-mediated imaging is one such technique. There are many appealing properties of nanoparticle-mediated molecular and cellular imaging, which include early detection, the ability to exploit the EPR effect in the case of tumors[1], long lasting contrast enhancement[1], and multiple imaging capabilities within one nanoplatform[1,18]. Also, recent advancements in this branch of research have resulted in the ability to design polymeric nanoparticle platforms that bioeliminate naturally from the body[19], further underscoring the advantages of nanoparticle-mediated imaging. Some notable examples of nanoparticle-mediated imaging include photoacoustic

[20-22], Raman [20,21], dark field [22], computed tomography and positron emission tomography (CT & PET) [23,24], and magnetic resonance imaging (MRI) [20,23] .

In addition, it is oftentimes quite crucial to perform imaging immediately after the administration of therapy, to monitor treatment efficacy, or in the case of cancer, to monitor the presence of residual tumor tissue and/or regrowth. Such imaging enables the clinician to monitor the efficacy and/or the need for further treatment. One example in which post-treatment imaging is crucial is exogenous cell therapy. Exogenous cell therapy, the use of transplanted cells to either totally replace or rejuvenate diseased cells, is a treatment modality that has been developed over the last 50 years. Recently, it has received more attention due to advances in stem cell research. Cell therapy has been utilized in the treatment of diseases or injuries associated with the teeth[25], central nervous system[26], and with autoimmune deficiency[27]. In order to continue to improve cell therapy techniques, applications, and overall efficacy, real time monitoring of the transplanted cells is crucial. Dyes, fluorescent proteins, quantum dots and genetic markers have all been utilized for monitoring transplanted cells. [28] Nanoparticle-mediated imaging, in this instance, has also gained interest because of the ability to tailor the nanoparticles for the specific cell line/therapy through the choice of matrix, physical properties, and surface characteristics. A review by Xu, *et al* [29] details the various nanoparticle imaging modalities, including fluorescence, MRI, and positron emission tomography, that have been successfully utilized in the tracking of implanted cells in animals and humans.

Additionally, the inclusion of nanoparticles can be used to strategically enhance the sensitivity and effectiveness of the conventional imaging method. A research effort led by Popovtzer[30] utilized targeted gold nanoparticles for molecular CT imaging of head and neck cancer lines, in conjunction with a clinical CT machine. The study demonstrated that because of the increased X-ray attenuation by the nanoparticles, the cancer cells to which the nanoparticles attached are easily detected and distinguished from noncancerous cells and cells that had not been treated with nanoparticles[30]. This study is an example of how the inclusion of nanoparticles can greatly enhance the information clinicians can attain without the need of purchasing more equipment or dramatically changing the treatment protocol.

1.1.3 Nanoparticle-Mediated Therapy

In the category of nanoparticle-mediated therapies, targeted drug delivery, photothermal, and photodynamic therapies have emerged as particularly promising among many other forms. A major advantage of nanoparticle-mediated therapy is the ability to selectively target malignant cells while leaving nearby healthy cells almost completely unharmed. Nanoparticle-mediated therapy enables a treatment option in which very low overall concentrations of a therapeutic agent are administered; however, the accumulation of the agent in the target cells is usually much higher than what can be achieved through intravenous administration of the drug alone, culminating in a much improved treatment efficacy and dramatically decreased rate of unwanted side-effects.

The large increase in treatment efficacy is primarily due to the inclusion of the therapeutic agent into the nanoparticle matrix, which is generally a targetable, biologically compatible, drug delivery vehicle. To date, nanoparticle-mediated therapy has been shown to be effective in addressing oncological [31-33], cardiovascular [34-36] and dermatological [37-39] ailments among other diseases. As a result, there continues to be a tremendous amount of interdisciplinary research effort driven by the promise of nanoparticle-mediated therapy and the dire need to understand the resulting physiological implications of this class of treatments.

1.1.1.a *Targeted Drug Delivery*

Targeted drug delivery via nanoparticles provides a treatment option with much less probability of unwanted side effects commonly associated with exposure to high doses of many drugs. An ideal treatment would improve the patient's standard of living, rather than further compromising their well-being, which may be declining due to the disease. Unfortunately, many of the most effective drugs for addressing severe and debilitating conditions also have acute side effects. The prospect of harsh side effects may make the decision between various treatments difficult. Chemotherapy, for example, is still one of the most widely utilized conventional cancer treatment methods, however, because these drugs typically target cells that divide rapidly, a common trait of many cancerous cells lines, any healthy cells that also share this trait are harshly damaged. According to the American Cancer Society, the most common side effects of chemotherapy include: damage to bone marrow, blood, hair follicle, digestive

tract, and reproductive tract cells. One innovative method to avoid these side effects is the encapsulation of the chemotherapy drug into a targeted nanoparticle matrix, to ensure that healthy cells do not interact with the drug. Furthermore, nanoparticle-mediated drug delivery enables the successful delivery of drugs to solid tumors by taking advantage of the enhanced permeability and retention effect[40], as well as of active targeting. Metal, polymeric, hybrids of metal and polymeric, and silica nanoparticles, are all currently being utilized for targeted chemotherapeutic drug delivery. [1, 32, 33, 41] Recently, for example, significant work in this area was completed by Liu et al.,[32] in which they describe the development of targeted silica nanoparticles that have a hydrophobic anticancer drug, docetaxel attached. A mixed layer of phospholipids served as a coating on the nanoparticles to ensure that the docetaxel did not interact with healthy cells. This particular study is representative of the essential benefits of targeted nanoparticle-mediated drug delivery, in that the study combines high drug loading, controlled drug release (pH), low toxicity and high efficacy in one treatment mode[32]. Another recent *in vivo* study, on ovarian cancer, demonstrates how targeted nanoparticles delivering the classical chemotherapeutic drug cisplatin work well even on tumors that are resistant to the "naked" cisplatin drug.[42]

1.1.1.b *Photothermal Therapy*

Nanoparticle-mediated photothermal therapy involves the selective heating of malignant cells while leaving the neighboring cells intact. Nanoparticle-

mediated photothermal therapy enables selective extracellular heating of the cells by attaching predominantly to the target cells external membranes or intracellular heating once the nanoparticle has been taken up within the cell. Successful nanoparticle-mediated photothermal therapy has been demonstrated with a variety of different types of nanoparticle matrices, encouraging continuous research efforts and applications. [43,44] Nanoparticle-mediated photothermal therapy is especially well suited for treating cancer due to the increased heat sensitivity associated with cancer cells, as well as a tumor's inability to efficiently dissipate heat as a result of the poor vasculature networks. Nanoparticle-mediated photothermal therapy has been used widely as both a primary mode of treatment as well as a preliminary treatment to weaken otherwise resistant cells to more conventional therapies.[17, 18, 43, 45]

1.1.1.c *Photodynamic Therapy*

Another emerging form of nanoparticle-mediated treatment is photodynamic therapy. Much like the previously discussed therapies, the need to encapsulate the therapeutic agent, in this case a photosensitizer, inside of a dynamic carrier is also of importance because many of the most widely used photosensitizers are hydrophobic and very susceptible to reduction into an inactive chemical form if administered intravenously. Furthermore, targeted delivery is also crucial to ensure that the reactive oxygen species that are produced following the excitation of the photosensitizer do not harm healthy cells. Many nanoparticle matrices have been utilized in photodynamic therapy studies

including ceramic, hydrogel, polymer/metal hybrid, and silica [1, 46 -50] A recent study conducted by Rojnik, et al [51], characterized the performance of FDA approved, PEGylatd poly-($_{D,L}$-lactide-co-glycolide) nanoparticles loaded with an extremely potent photosensitizer, temporfin in both *in vitro* and *in vivo* studies. The researchers demonstrated that controlled release of the photosensitizer to target cells could successfully be controlled, via the modification of the nanoparticles' composition, pore size, and surfaces. Additionally, the study demonstrated that the incorporation of the photosensitizer into the nanoparticle matrix resulted in an increase in photodynamic effectiveness *in vitro* when compared to its administration in a standard solution and an advantageous distribution throughout the tumors in the *in vivo* studies. [51]

1.2 Overview of This Dissertation

Chapter 2 of this dissertation describes the first ever use of Coomassie Brilliant Blue G-250 dye as therapeutic agent for photothermal therapy. Coomassie blue dye has various desirable qualities. It is a derivative of the commonly used food coloring Blue No. 1 and is nontoxic to healthy animals at very high concentrations. The dye also has a very high molar absorption coefficient at 600nm and nearly no fluorescence quantum yield. Taken together, Coomassie blue dye is an ideal candidate for use as a photothermal therapy agent as it can be utilized at high concentrations to absorb strongly in the therapeutic window (wavelengths ranging from 600-1000nm) and reradiate the absorbed energy predominately in the form of heat to the surrounding

environment. **Chapter 2** details a study in which the dye has been covalently linked into a polyacrylamide nanoparticle matrix and utilized in *in vitro* experiments with HeLa cells. This study establishes a third mode of application for this specific type of nanoparticles as they have also been used successfully in visual delineation [2,52-54] and photoacoustic imaging studies[18] of brain tumors, previously performed in the Kopelman lab.

Chapter 3 details the optimization of gold nanoparticles, fabricated using femtosecond laser ablation, for nuclear delivery into HeLa cells. Among the large variety of subcellular organelles, the nucleus remains a significant target for nanoparticle research, i.e. investigations of potential diagnostic and therapeutic applications, due mostly to the genetic information and transcription machinery, which reside there. Gold nanoparticles manufactured via laser ablation of a bulk gold in ultra pure water yields so called “virgin surfaces” devoid of any unreacted chemical molecules, as is the case of chemical, wet lab techniques for producing gold nanoparticles. These virgin surfaces enable the optimization for intracellular and subsequent nuclear delivery through the addition of peptides. In the study outlined in **Chapter 3**, two peptides, RGD & NLS, were attached to the nanoparticles and successful, efficient nuclear delivery was achieved using a nanoparticle concentration of only 100pM.

Some forms of gold nanoparticle-mediated photothermal therapy are advantageous over other forms of nanoparticle-mediated photothermal therapy, due to their ability to take advantage of the “therapeutic window” in which one utilizes near-infrared (NIR) radiation to excite the Au NPs and induce thermolysis

in cells. Single gold nanoparticles have a maximum absorption in the range of 520-560nm. When irradiated at these wavelengths, the electrons are photoexcited and they vibrate, which in turn produces heat. This heat production is exploited in gold nanoparticle mediated photothermal therapy. The localized heating due to the nanoparticles within the cell leads to hyperthermia, photothermal lysis and cell death. Photothermal therapy proved to be an attractive alternative to conventional treatments for many reasons; one of the most important reasons is that cancer cells are known to be more heat sensitive than normal, healthy cells. Despite several successful experimental demonstrations of this technique, a complete theoretical treatment did not emerge until much later. Khlebtsov, et al describe the temperature change due to irradiating *solid*, single gold nanoparticles, as well as various types of clusters. A brief summary for single gold nanoparticle follows; a more detailed treatment is given in Chapter 4. The change in temperature as a result of heating a single gold nanoparticle in water can be described as follows,

$$\Delta T = \frac{<F>C_{abs}}{\kappa m} \qquad \textbf{Eqn. 1.1}$$

where <F> is the average laser fluence, C_{abs} is the absorption cross section, m is the mass of the gold nanoparticle, and κ is the specific heat of gold, and r is the radius of the nanoparticle. If the dimensionless quantity, Q_{abs}, is defined as the normalized absorption cross-section and use the density of gold, ρ, Eqn. 1.1 can be rewritten as:

$$\Delta T = \frac{<F>Q_{abs}}{\kappa \rho r}$$ **Eqn. 1.2**

The fraction of C_{abs}/m or Q_{abs}/r determine the heating and therefore the efficiency with which one can kill the cell. These fractions explain the reason that gold nanorod-mediated photothermal therapy is more effective in some respects. However, it is important to note that this method has drawbacks including increased dark toxicity, and occasional changes in nanoparticle morphology due to melting and thermal stress, which results in a shift of the absorption spectrum.

Encouraged by the results of the previous study, the same nanoparticles described in **Chapter 3** were utilized for photothermal therapy of HeLa cells. Chapter 4 is a comparative study of the efficacy of photothermal therapy when treatment is mediated by gold nanoparticles located predominantly within the nucleus in contrast to when the Au NPs are predominantly in the cytoplasm. The advantages of directly heating the nuclei of the cancer cells are numerous, including the smaller target volume, lower heat capacity and increased likelihood of causing irreparable damage to the cell's DNA (located in nucleus). Furthermore, it is likely that nucleus specific PTT will induce notable differences in the mechanisms through which the cancer cell dies, which will provide invaluable insight for *in vivo* treatment planning. **Chapter 4** describes a systematic study of the difference in PTT efficacy over short- and long-term time periods when the Au NPs are targeted and efficiently delivered to the cancer cell

nuclei as well as some discussion of the pathways throughout the cells die in both scenarios.

1.3 Figures

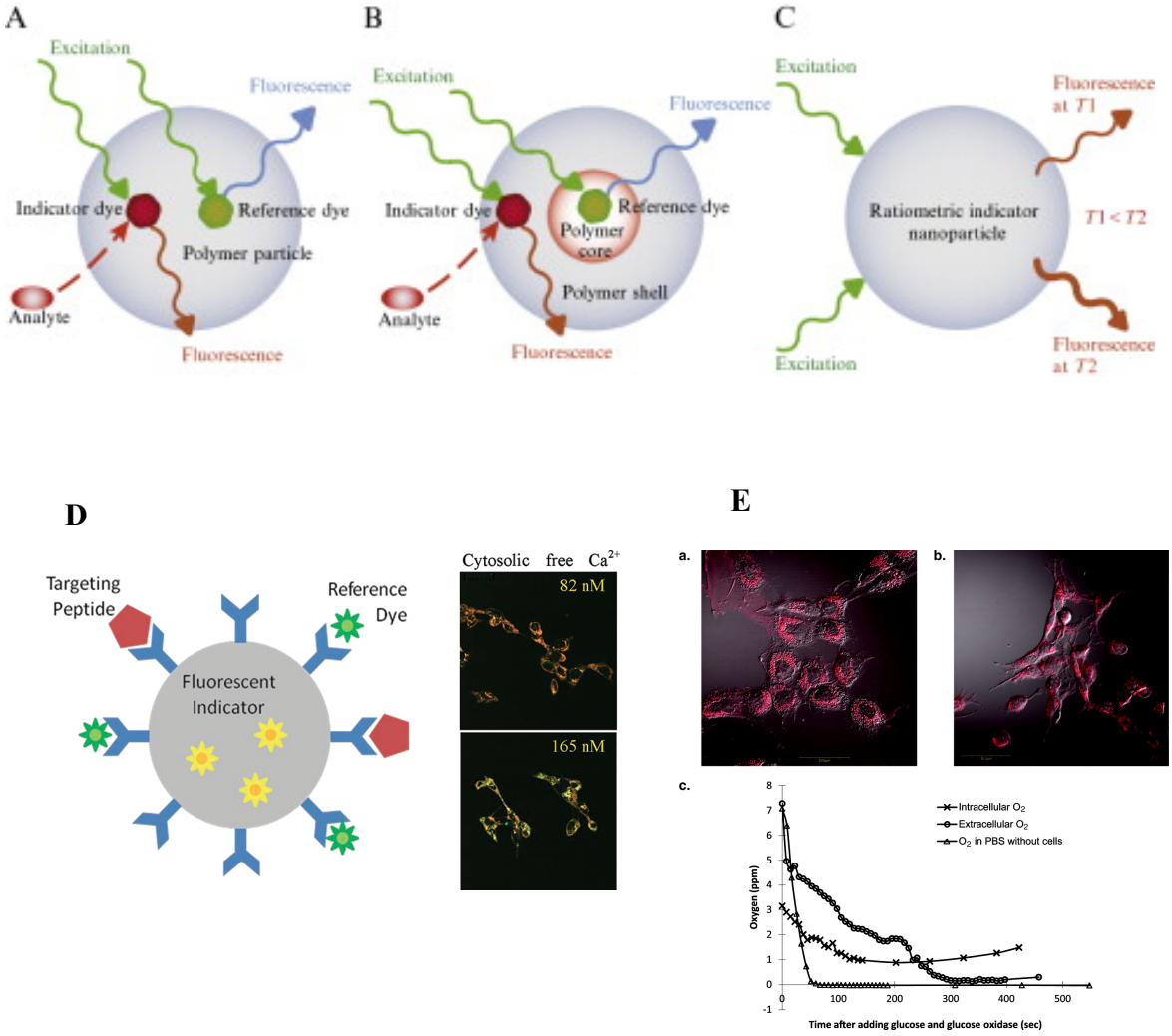

Figure 1.1: Schematics PEBBLE sensors [55] : (A) Single core NP loaded with both sensing and reference components), (B) Core–shell PEBBLE (core–shell NPs with spatially separated sensing and reference components), (C) Temperature-sensitive NP PEBBLE (NP matrix as a sensing unit). PEBBLE-mediated studies [8 17] : (D) Intracellular Ca^{2+} and (E) oxygen sensing.

1.4 References

1. Koo, Y. E. L.; Reddy, G. R.; Bhojani, M.; Schneider, R.; Philbert, M. A.; Rehemtulla, A.; Ross, B. D.; Kopelman, R., Brain cancer diagnosis and therapy with nanoplatforms. *Advanced Drug Delivery Reviews* **2006,** *58* (14), 1556-1577.

2. Orringer, D. A.; Chen, T.; Huang, D. L.; Armstead, W. M.; Hoff, B. A.; Koo, Y. E. L.; Keep, R. F.; Philbert, M. A.; Kopelman, R.; Sagher, O., The Brain Tumor Window Model: A Combined Cranial Window and Implanted Glioma Model for Evaluating Intraoperative Contrast Agents. *Neurosurgery* **2010,** *66* (4), 736-743.

3. Brakmane, G.; Winslet, M.; Seifalian, A. M., Systematic review: the applications of nanotechnology in gastroenterology. *Alimentary Pharmacology & Therapeutics* **2012,** *36* (3), 213-221.

4. Zhang, Y.; Zhou, D. J., Magnetic particle-based ultrasensitive biosensors for diagnostics. *Expert Review of Molecular Diagnostics* **2012,** *12* (6), 565-571.

5. Kinnunen, P.; McNaughton, B. H.; Albertson, T.; Sinn, I.; Mofakham, S.; Elbez, R.; Newton, D. W.; Hunt, A.; Kopelman, R., Self-Assembled Magnetic Bead Biosensor for Measuring Bacterial Growth and Antimicrobial Susceptibility Testing. *Small* **2012,** *8* (16), 2477-2482.

6. Sinn, I.; Albertson, T.; Kinnunen, P.; Breslauer, D. N.; McNaughton, B. H.; Burns, M. A.; Kopelman, R., Asynchronous Magnetic Bead Rotation Microviscometer for Rapid, Sensitive, and Label-Free Studies of Bacterial Growth and Drug Sensitivity. *Analytical Chemistry* **2012,** *84* (12), 5250-5256.

7. Multifunctional Nanoparticles for Drug Delivery Applications: Imaging, Targeting, and Delivery. *Multifunctional Nanoparticles for Drug Delivery Applications: Imaging, Targeting, and Delivery* **2012**, 1-373.

8. Si, D.; Epstein, T.; Lee, Y. E. K.; Kopelman, R., Nanoparticle PEBBLE Sensors for Quantitative Nanomolar Imaging of Intracellular Free Calcium Ions. *Analytical Chemistry* **2012,** *84* (2), 978-986.

9. Clark, H. A.; Kopelman, R.; Tjalkens, R.; Philbert, M. A., Optical nanosensors for chemical analysis inside single living cells. 2. Sensors for pH and calcium and the intracellular application of PEBBLE sensors. *Analytical Chemistry* **1999,** *71* (21), 4837-4843.

10. Clark, H. A.; Hoyer, M.; Philbert, M. A.; Kopelman, R., Optical nanosensors for chemical analysis inside single living cells. 1. Fabrication, characterization, and methods for intracellular delivery of PEBBLE sensors. *Analytical Chemistry* **1999,** *71* (21), 4831-4836.

11. Brasuel, M.; Kopelman, R.; Aylott, J. W.; Clark, H.; Xu, H.; Hoyer, M.; Miller, T. J.; Tjalkens, R.; Philbert, M. A., Production, characteristics and applications of fluorescent PEBBLE nanosensors: Potassium, oxygen, calcium and pH imaging inside live cells. *Sensors and Materials* **2002,** *14* (6), 309-338.

12. Koo, Y. E. L.; Cao, Y. F.; Kopelman, R.; Koo, S. M.; Brasuel, M.; Philbert, M. A., Real-time measurements of dissolved oxygen inside live cells by organically modified silicate fluorescent nanosensors. *Analytical Chemistry* **2004,** *76* (9), 2498-2505.

13. Brasuel, M.; Kopelman, R.; Miller, T. J.; Tjalkens, R.; Philbert, M. A., Fluorescent nanosensors for intracellular chemical analysis: Decyl methacrylate liquid polymer matrix and ion exchange-based potassium PEBBLE sensors with real-time application to viable rat C6 glioma cells. *Analytical Chemistry* **2001,** *73* (10), 2221-2228.

14. Sumner, J. P.; Aylott, J. W.; Monson, E.; Kopelman, R., A fluorescent PEBBLE nanosensor for intracellular free zinc. *Analyst* **2002,** *127* (1), 11-16.

15. Brasuel, M. G.; Miller, T. J.; Kopelman, R.; Philbert, M. A., Liquid polymer nano-PEBBLEs for Cl- analysis and biological applications. *Analyst* **2003,** *128* (10), 1262-1267.

16. Xu, H.; Aylott, J. W.; Kopelman, R.; Miller, T. J.; Philbert, M. A., A real-time ratiometric method for the determination of molecular oxygen inside living cells using sol-gel-based spherical optical nanosensors with applications to rat C6 glioma. *Analytical Chemistry* **2001,** *73* (17), 4124-4133.

17. Lee, Y.-E. K.; Ulbrich, E. E.; Kim, G.; Hah, H.; Strollo, C.; Fan, W.; Gurjar, R.; Koo, S. M.; Kopelman, R., Near Infrared Luminescent Oxygen Nanosensors with Nanoparticle Matrix Tailored Sensitivity. *Analytical Chemistry* **2010,** *82* (20), 8446-8455.

18. Ray, A.; Wang, X. D.; Lee, Y. E. K.; Hah, H. J.; Kim, G.; Chen, T.; Orringer, D. A.; Sagher, O.; Liu, X. J.; Kopelman, R., Targeted blue nanoparticles as photoacoustic contrast agent for brain tumor delineation. *Nano Research* **2011,** *4* (11), 1163-1173.

19. Wang, S. Y.; Fan, W. Z.; Kim, G.; Hah, H. J.; Lee, Y. E. K.; Kopelman, R.; Ethirajan, M.; Gupta, A.; Goswami, L. N.; Pera, P.; Morgan, J.; Pandey, R. K., Novel Methods to Incorporate Photosensitizers Into Nanocarriers for Cancer Treatment by Photodynamic Therapy. *Lasers in Surgery and Medicine* **2011,** *43* (7), 686-695.

20. Kircher, M. F.; de la Zerda, A.; Jokerst, J. V.; Zavaleta, C. L.; Kempen, P. J.; Mittra, E.; Pitter, K.; Huang, R. M.; Campos, C.; Habte, F.; Sinclair, R.; Brennan, C. W.; Mellinghoff, I. K.; Holland, E. C.; Gambhir, S. S., A brain tumor molecular imaging strategy using a new triple-modality MRI-photoacoustic-Raman nanoparticle. *Nature Medicine* **2012,** *18* (5), 829-U235.

21. Wang, C.; Ma, X. X.; Ye, S. Q.; Cheng, L.; Yang, K.; Guo, L.; Li, C. H.; Li, Y. G.; Liu, Z., Protamine Functionalized Single-Walled Carbon Nanotubes for Stem Cell Labeling and In Vivo Raman/Magnetic Resonance/Photoacoustic Triple-Modal Imaging. *Advanced Functional Materials* **2012,** *22* (11), 2363-2375.

22. Priyam, A.; Idris, N. M.; Zhang, Y., Gold nanoshell coated NaYF4 nanoparticles for simultaneously enhanced upconversion fluorescence and darkfield imaging. *Journal of Materials Chemistry* **2012,** *22* (3), 960-965.

23. Hahn, M. A.; Singh, A. K.; Sharma, P.; Brown, S. C.; Moudgil, B. M., Nanoparticles as contrast agents for in-vivo bioimaging: current status and future perspectives. *Analytical and Bioanalytical Chemistry* **2011,** *399* (1), 3-27.

24. Huang, F. Y. J.; Lee, T. W.; Kao, C. H. K.; Chang, C. H.; Zhang, X. N.; Lee, W. Y.; Chen, W. J.; Wang, S. C.; Lo, J. M., Imaging, Autoradiography, and Biodistribution of Re-188-Labeled PEGylated Nanoliposome in Orthotopic Glioma

Bearing Rat Model. *Cancer Biotherapy and Radiopharmaceuticals* **2011,** *26* (6), 717-725.

25. Ahangari, Z.; Naseri, M.; Jalili, M.; Mansouri, Y.; Mashhadiabbas, F.; Torkaman, A., Effect of Propolis on Dentin Regeneration and the Potential Role of Dental Pulp Stem Cell in Guinea Pigs. *Cell Journal* **2012,** *13* (4), 223-228.

26. Khalili, M. A.; Anvari, M.; Hekmati-Moghadam, S. H.; Sadeghian-Nodoushan, F.; Fesahat, F.; Miresmaeili, S. M., Therapeutic Benefit of Intravenous Transplantation of Mesenchymal Stem Cells After Experimental Subarachnoid Hemorrhage in Rats. *Journal of Stroke & Cerebrovascular Diseases* **2012,** *21* (6), 445-451.

27. Francois, M.; Galipeau, J., New insights on translational development of mesenchymal stromal cells for suppressor therapy. *Journal of Cellular Physiology* **2012,** *227* (11), 3535-3538.

28. Blits, B.; Kitay, B. M.; Sanchez, A. R.; Andrade, C. M.; Pearse, D. D., 662. The Tracking of Exogenous Cells in the Injured Central Nervous System: Viral Vector Labeling Versus an Intrinsic Genetic Marker. *Mol Ther* **2005,** *11* (S1), S256-S256.

29. Xu, C. J.; Mu, L. Y.; Roes, I.; Miranda-Nieves, D.; Nahrendorf, M.; Ankrum, J. A.; Zhao, W. A.; Karp, J. M., Nanoparticle-based monitoring of cell therapy. *Nanotechnology* **2011,** *22* (49).

30. Popovtzer, R.; Agrawal, A.; Kotov, N. A.; Popovtzer, A.; Balter, J.; Carey, T. E.; Kopelman, R., Targeted Gold Nanoparticles Enable Molecular CT Imaging of Cancer. *Nano Letters* **2008,** *8* (12), 4593-4596.

31. Xie, J.; Liu, G.; Eden, H. S.; Ai, H.; Chen, X., Surface-Engineered Magnetic Nanoparticle Platforms for Cancer Imaging and Therapy. *Accounts of Chemical Research* **2011,** *44* (10), 883-892.

32. Liu, Y.; Mi, Y.; Zhao, J.; Feng, S.-S., Multifunctional silica nanoparticles for targeted delivery of hydrophobic imaging and therapeutic agents. *International Journal of Pharmaceutics* **2011,** *421* (2), 370-378.

33. Peng, X.-H.; Wang, Y.; Huang, D.; Wang, Y.; Shin, H. J.; Chen, Z.; Spewak, M. B.; Mao, H.; Wang, X.; Wang, Y.; Chen, Z.; Nie, S.; Shin, D. M., Targeted Delivery of Cisplatin to Lung Cancer Using ScFvEGFR-Heparin-Cisplatin Nanoparticles. *Acs Nano* **2011,** *5* (12), 9480-9493.

34. Lobatto, M. E.; Fuster, V.; Fayad, Z. A.; Mulder, W. J. M., Perspectives and opportunities for nanomedicine in the management of atherosclerosis. *Nature Reviews Drug Discovery* **2011,** *10* (11), 835-852.

35. McCarthy, J. R., Multifunctional agents for concurrent imaging and therapy in cardiovascular disease. *Advanced Drug Delivery Reviews* **2010,** *62* (11), 1023-1030.

36. Fishbein, I.; Chorny, M.; Levy, R. J., Site-specific gene therapy for cardiovascular disease. *Current Opinion in Drug Discovery & Development* **2010,** *13* (2), 203-213.

37. El-Sayed, I. H.; Huang, X. H.; El-Sayed, M. A., Selective laser photo-thermal therapy of epithelial carcinoma using anti-EGFR antibody conjugated gold nanoparticles. *Cancer Letters* **2006,** *239* (1), 129-135.

38. Choi, J.; Yang, J.; Bang, D.; Park, J.; Suh, J. S.; Huh, Y. M.; Haam, S., Targetable Gold Nanorods for Epithelial Cancer Therapy Guided by Near-IR Absorption Imaging. *Small* **2012,** *8* (5), 746-753.

39. Bauer, B.; Chen, S.; Kall, M.; Gunnarsson, L.; Ericson, M. B. In *Metal nanoparticles amplify photodynamic effect on skin cells in vitro*, Conference on Optical Interactions with Tissue and Cells XXII, San Francisco, CA, Jan 24-26; San Francisco, CA, **2011**.

40. Konan, Y. N.; Gurny, R.; Allemann, E., State of the art in the delivery of photosensitizers for photodynamic therapy. *Journal of Photochemistry and Photobiology B-Biology* **2002,** *66* (2).

41. Papasani, M. R.; Wang, G.; Hill, R. A., Gold nanoparticles: the importance of physiological principles to devise strategies for targeted drug delivery. *Nanomedicine: Nanotechnology, Biology and Medicine* **2012,** *8* (6), 804-814.

42. Winer, I.; Wang, S. Y.; Lee, Y. E. K.; Fan, W. Z.; Gong, Y. S.; Burgos-Ojeda, D.; Spahlinger, G.; Kopelman, R.; Buckanovich, R. J., F3-Targeted Cisplatin-Hydrogel Nanoparticles as an Effective Therapeutic That Targets Both Murine and Human Ovarian Tumor Endothelial Cells In vivo. *Cancer Research* **2010,** *70* (21), 8674-8683.

43. Norman, R. S.; Stone, J. W.; Gole, A.; Murphy, C. J.; Sabo-Attwood, T. L., Targeted photothermal lysis of the pathogenic bacteria, Pseudomonas aeruginosa, with gold nanorods. *Nano Letters* **2008,** *8* (1), 302-306.

44. Iancu, C.; Mocan, L., Advances in cancer therapy through the use of carbon nanotube-mediated targeted hyperthermia. *International Journal of Nanomedicine* **2011,** *6*.

45. Kirui, D. K.; Rey, D. A.; Batt, C. A., Gold hybrid nanoparticles for targeted phototherapy and cancer imaging. *Nanotechnology* **2010,** *21* (10).

46. Roy, I.; Ohulchanskyy, T. Y.; Pudavar, H. E.; Bergey, E. J.; Oseroff, A. R.; Morgan, J.; Dougherty, T. J.; Prasad, P. N., Ceramic-based nanoparticles entrapping water-insoluble photosensitizing anticancer drugs: A novel drug-carrier system for photodynamic therapy. *Journal of the American Chemical Society* **2003,** *125* (26), 7860-7865.

47. Hah, H. J.; Kim, G.; Lee, Y.-E. K.; Orringer, D. A.; Sagher, O.; Philbert, M. A.; Kopelman, R., Methylene Blue-Conjugated Hydrogel Nanoparticles and Tumor-Cell Targeted Photodynamic Therapy. *Macromolecular Bioscience* **2011,** *11* (1).

48. Qin, M.; Hah, H. J.; Kim, G.; Nie, G.; Lee, Y.-E. K.; Kopelman, R., Methylene blue covalently loaded polyacrylamide nanoparticles for enhanced tumor-targeted photodynamic therapy. *Photochemical & Photobiological Sciences* **2011,** *10* (5).

49. Gary-Bobo, M.; Mir, Y.; Rouxel, C.; Brevet, D.; Hocine, O.; Maynadier, M.; Gallud, A.; Da Silva, A.; Mongin, O.; Blanchard-Desce, M.; Richeter, S.; Loock, B.; Maillard, P.; Morere, A.; Garcia, M.; Raehm, L.; Durand, J.-O., Multifunctionalized mesoporous silica nanoparticles for the in vitro treatment of

retinoblastoma: Drug delivery, one and two-photon photodynamic therapy. *International Journal of Pharmaceutics* **2012,** *432* (1-2).

50. Reddy, G. R.; Bhojani, M. S.; McConville, P.; Moody, J.; Moffat, B. A.; Hall, D. E.; Kim, G.; Koo, Y. E. L.; Woolliscroft, M. J.; Sugai, J. V.; Johnson, T. D.; Philbert, M. A.; Kopelman, R.; Rehemtulla, A.; Ross, B. D., Vascular targeted nanoparticles for imaging and treatment of brain tumors. *Clinical Cancer Research* **2006,** *12* (22), 6677-6686.

51. Rojnik, M.; Kocbek, P.; Moret, F.; Compagnin, C.; Celotti, L.; Bovis, M. J.; Woodhams, J. H.; MacRobert, A. J.; Scheglmann, D.; Helfrich, W.; Verkaik, M. J.; Papini, E.; Reddi, E.; Kos, J., In vitro and in vivo characterization of temoporfin-loaded PEGylated PLGA nanoparticles for use in photodynamic therapy. *Nanomedicine* **2012,** *7* (5).

52. Orringer, D. A.; Koo, Y. E. L.; Chen, T.; Kim, G.; Hah, H. J.; Xu, H.; Wang, S. Y.; Keep, R.; Philbert, M. A.; Kopelman, R.; Sagher, O., In vitro characterization of a targeted, dye-loaded nanodevice for intraoperative tumor delineation. *Neurosurgery* **2009,** *64* (5), 965-971.

53. Orringer, D. A.; Koo, Y. E.; Chen, T.; Kopelman, R.; Sagher, O.; Philbert, M. A., Small Solutions for Big Problems: The Application of Nanoparticles to Brain Tumor Diagnosis and Therapy. *Clinical Pharmacology & Therapeutics* **2009,** *85* (5), 531-534.

54. Nie, G. C.; Hah, H. J.; Kim, G.; Lee, Y. E. K.; Qin, M.; Ratani, T. S.; Fotiadis, P.; Miller, A.; Kochi, A.; Gao, D.; Chen, T.; Orringer, D. A.; Sagher, O.; Philbert, M. A.; Kopelman, R., Hydrogel Nanoparticles with Covalently Linked

Coomassie Blue for Brain Tumor Delineation Visible to the Surgeon. *Small* **2012,** *8* (6), 884-891.

55. Lee, Y. E. K.; Kopelman, R., Nanoparticle PEBBLE Sensors in Live Cells. *Imaging and Spectroscopic Analysis of Living Cells: Optical and Spectroscopic Techniques* **2012,** *504*, 419-470.

Chapter 2 Photothermal Therapy of Cancer Cells Mediated by Blue Hydrogel Nanoparticles

Some of the material in this chapter has been adapted with minor modifications from the following article, which has been accepted for publication:

Curry, T., Epstein, T., Smith, R., & Kopelman, R. Photothermal Therapy of Cancer Cells mediated by Blue Hydrogel Nanoparticles. Nanomedicine, (2012). *Accepted for publication*

2.1 Introduction

Cancer is still one of the leading causes of death in America; in 2010, 1,596,670 new cases and 571,950 cancer-related deaths were projected to occur[1]. To address this challenge, many advances have been made in the early detection and treatment, directly resulting in an increase in the treatment options available including chemotherapy, radiation treatment, and surgical removal. Despite these advances, cancer treatment has continued to be a hotbed of research because in many instances treatment plans must be robust to address the issues of probable damage to surrounding healthy tissues, tumor regrowth, and a decrease in the quality of life for the patient. In recent years many groups have devoted their efforts toward employing nanoparticle (NP) platforms for detecting and treating various types of cancer. Nanoparticles are advantageous

because they are minimally invasive, have tunable characteristics (i.e. size, absorption, surface charge), and can be used as targeted, multifunctional, or combined treatment platforms[2-4]. To date, nanoparticles have been used as contrast agents for the detection and imaging of cancerous cells, both in vitro and in vivo, coupled with photosynthesizing dyes for photodynamic therapy, or combined with chemotherapy drugs to facilitate cell specific drug delivery, as well as coupled with external magnetic fields to induce cell death via hyperthermia[2-10].

Photothermal therapy (PTT) mediated by nanoparticles has emerged as a promising cancer treatment modality that has been used to treat various cancerous cell lines. Gold, silver, iron oxide, and magnetite are some of the materials that have been used in nanoparticle mediated PTT[10-13]. Of these, the use of gold nanoparticles has seemingly emerged as the frontrunner in PTT research and various groups have created experimental protocols that yield a large variety in the gold nanoparticle structures, including nanorods, triangles, pyramids, and shells[10,12]. Many groups utilize NIR radiation to excite the gold nanoparticles and induce thermolysis in cells, taking advantage of the low absorption and scattering of the radiation by tissues at these wavelengths. Despite these advantages, there have been many studies conducted exploring the origins and levels of cytotoxicity of many types of gold nanostructures, with apparently conflicting conclusions regarding their use[8,14,15]. This, and other considerations (see below), may be opening the door for assessing the potential of another PTT modality aimed at a widespread use in the treatment of various malignant cancers. Notably, polymeric nanoparticles have been FDA approved

for clinical studies due to their apparent high therapeutic factor[16]. In particular, much research has been done on biocompatible, biodegradable, and bio-eliminable hydrogel nanoparticle platforms[3,4]. Incorporated for this study is the FDA approved dye, Coomassie blue.

In this study we investigate the utility of biologically compatible hydrogel nanoparticles, which have Coomassie blue (CB) dye covalently linked into their polyacrylamide (PAA) matrix, called here CB-PAA, as candidates for photothermal therapy (PTT) of cancer cells *in vitro.* We substantiated the capability of the CB-PAA nanoparticles to serve as a platform for a multimodal therapeutic approach (photoacoustic imaging[20], visual surgical delineation[17-19], and now PTT). Nanoparticles of this type have previously been used in our lab for **targeted** *in vivo* photodynamic therapy (with photosensitizers such as methylene blue), combined with MRI and EPR contrast enhancement agents, as well as for photoacoustic structural imaging and for the delineation of glioma boundaries (in the latter two cases with CB-PAA NPs, detailed in the background section), and have also been shown to be non-toxic, targetable, biodegradable and bio-eliminable[17-20]. Thus, with the here demonstrated use for PTT, such CB-PAA NPs would be utilizable in three different ways, even simultaneously, i.e. tri-functional, to which can easily be added targetability.

The simplicity of the method described here goes beyond the use of existing nano-platforms. The excitation source employed in this study is an inexpensive, portable LED array with a maximum emission at 590 nm. Based on its use we find that CB-PAA mediated PTT of HeLa cells, incubated with 1.2

mg/mL of nanoparticles for 24 hours, yields nearly complete cell death, within 1 hour of treatment, after 40 minutes of illumination. Moreover, cells that were incubated for 24 hours with only 0.6mg/mL of the nanoparticles, and with only 20 minutes of illumination, yielded nearly complete cell death 3 hours after treatment. On the other hand, under identical illumination, but without incorporation of the dye, there is little cell kill. Likewise, with no illumination, but with the dye containing NPs, there is insignificant cell kill. This promises, for in-vivo use, an extremely high selectivity of cell death, based on combined immuno and "illumo" targeting, with minimal side effects. Overall, we find that CB-PAA mediated PTT is characterized by high efficacy, with much promise for inclusion in a multi-pronged and safe approach for treating various types of cancers.

2.1.1 Background

As previously mentioned, CB-PAA nanoparticles were utilized in two previous studies. The first study[19] detailed: 1) the development of a derivatized CB-APMA—an acrylamide terminated form of the commercially available CB dye, 2) the preparation of covalently linked CB-PAA using the crosslinkable CB derivative, and 3) surface modification of the CB-PAA nanoparticles with polyethylene glycol (PEG) and F3 peptide for improved biostability and decreased nonspecific binding. The development and incorporation of the crosslinkable CB derivative into the PAA nanoparticle matrix resulted in high dye loading efficiency (ca. 70 % of the input amount of CB), which is lower than PAA nanoparticles post-loaded with CB dye (ca. 90%), but much higher than the PAA

nanoparticles with encapsulated CB dye (ca. 5%). Dye leaching experiments conducted under simulated physiological conditions demonstrated that the CB-PAA nanoparticles were by far the best candidates for the delineation studies as no dye leaching was detected. On the other hand, between 50-70% of the CB dye leached out of the post-loaded nanoparticles within 2 hours. *In vitro* staining experiments conducted with targeted nanoparticles on 9L gliosarcoma cells demonstrated effective cell staining, while the blue color from the non-targeted cells was negligible. *In vivo* tumor delineation studies were conducted using rat BTW models with implanted 9L gliosarcomas and cranial windows. Rats treated with targeted, CB-PAA showed the increasing and longer lasting visual delineation (with no additional lighting, or optical aid required) up to 2 hours in comparison to the nanoparticles with CB post-loaded and encapsulated within the matrices.

The second study[20] involved the use of the surgically removed rat brains for photoacoustic imaging of the implanted tumors *ex vivo*. For imaging purposes, two brains from rats that were treated with different nanoparticle concentrations (250 mg/Kg and 125mg/Kg) and a control brain (no treatment), were placed together and imaged simultaneously. The tumor from the rat that was treated with the highest concentration of nanoparticles was clearly visible to the eye; however, the tumor from the rat that was treated with the lower nanoparticle concentration was not distinguishable from the surrounding healthy tissue. The photoacoustic image generated by the nanoparticles enabled

observation of both tumors and the control brain could not be seen in the image. The first two prongs of the multimodal, therapeutic approach was established in

2.2 Materials and Methods

2.2.1 Materials

Coomassie blue G (CB), acrylamide (AA), ammonium persulfate (APS), *N*,*N*,*N'*,*N'*-tetramethylethylenediamine (TEMED), sodium dioctyl sulfosuccinate (AOT), Brij 30, *N,N*-dimethylformamide (DMF), dimethyl sulfoxide (DMSO), and 3-(4,5-dimethylthiazolyl-2)-2,5-diphenyltetrazolium bromide (MTT) were purchased from Sigma Aldrich. Dulbecco's Modified Eagle medium (DMEM 1195 & 21063), Dulbecco's Phosphate Buffered Saline (DPBS), Rosewell Park Memorial Institute medium (RPMI-1640), fetal bovine serum (FBS), and penicillin-streptomycin glutamine, Live/Dead *Bac*light Bacterial Viability Kit, were all purchased from Invitrogen. *N*-(3-Aminopropyl) methacrylamide hydrochloride (APMA) was purchased from Polysciences Inc. Ethanol (95%), and hexane were purchased from Fisher Scientific. Phosphate buffered saline (PBS) solution (pH 7.4) was made with phosphate buffered saline tablet from Sigma Aldrich. 100mm, 35mm, and 96-well microplates were purchased from BD Biosciences. The water used throughout the experiment was deionized (DI) water, purified by a Milli-Q system from Millipore Co.

2.2.2 Light Source

The excitation source employed for the PTT experiments is a low intensity LED array created with an emission peak of 590nm. The array was fabricated in house as follows: an array of 256 wide angle LEDs from Kingbright Corporation were soldered to a fiberglass PCB board; wide angle LEDs and mirrors were then attached around the perimeter of the array to increase illumination uniformity, and lastly, an adjustable power supply was connected to the setup to enable control of the power output of the LED array. The intensity of the array is 25.4 mW/cm^2 and the deviation in irradiance at the face of the mirrors was found to be 6.2%.

2.2.3 Cell Culture

HeLa 229 cells (American Type Culture Collection) were grown in Dulbecco's modified Eagle medium (DMEM 11995) supplemented with 10% fetal bovine serum (FBS) and 1% penicillin-streptomycin at 37°C and 5% CO_2 in a humidified incubator. Cells were plated and grown in 100mm petri dishes for the cellular uptake assay, in 96 well plates for the MTT assay, and in 35mm petri dishes for the photothermal therapy tests.

2.2.4 Nanoparticle Synthesis & Characterization

2.2.4a Synthesis

The CB-PAA used in this study were synthesized according to a protocol established in a previous study completed in our group[17], and modified slightly

using the Coomassie blue derivative as the only cross-linker. Briefly, the Coomassie blue (CB) covalently linked polyacrylamide (PAA) nanoparticles were prepared by a reverse microemulsion polymerization method. A monomer solution was prepared by dissolving monomers, acrylamide (610 mg) and APMA (40mg), in 1.2mL of water. A dye solution was prepared by dissolving 165 mg of CB linked APMA in 0.8 mL of DMF and then 0.4-1.0mL of Brij 30 was added to the dye solution. The monomer and dye solutions were mixed and sonicated to make a homogeneous solution. The solution was then added to a deoxygenated hexane (60mL) that contained two surfactants, AOT (4.8 g) and Brij 30 (total amount of 9.5 mL). After stirring the mixture under inert atmosphere for 20 min, a freshly prepared 66% (w/v) APS solution (400 µL) and TEMED (200 µL) were added to the mixture solution to initiate polymerization. The solution was then stirred under inert atmosphere at room temperature for 1.5 hours. After completing the polymerization, hexane was removed with a Büch RII rotary evaporator and the residue was then suspended in ethanol. The suspension was then washed in an Amicon filtration system (Millipore Co.) with a 300,000 NMWL Millipore ultrafiltration membrane under 10-20 psi of pressure with ethanol 10 times followed by 10 water washes to ensure all surfactants and unreacted molecules were removed. The nanoparticle solution was then filtered through a 0.22 Whatman syringe filter. The resultant CB-PAA nanoparticles were freeze-dried and stored at room temperature in a Thermo Electron Corp ModulyoD freeze dryer for later use.

Blank PAA NPs were fabricated using the procedure outlined in a previous study conducted by our group[17]. Briefly, the blank PAA nanoparticles were also prepared by a reverse microemulsion polymerization method. A monomer solution was prepared by dissolving monomers, acrylamide (711 mg) and APMA (55 mg), in 1.6 mL of DPBS. GDMA (470 µL) was added to the monomer solution and then the mixture was stirred and sonicated to make a homogeneous solution. The monomer solution was added to a deoxygenated hexane (45 mL) that had been previously mixed with two surfactants, AOT (1.6 g) and Brij 30 (3.3 mL). The mixture was stirred under an inert atmosphere for at least 20 minutes, after which the initiators, 10% (w/v) APS solution (100 µL) and TEMED (100 µL), were added to begin polymerization. The solution was stirred under inert atmosphere at room temperature for at least 2 hours. The remaining hexane was removed with the rotary evaporator and ethanol was added to form a residue. The suspension was washed in an Amicon filtration system (Millipore) with a 300 kDa filter membrane under 10-20 psi of pressure with ethanol 5 times and with water 5 times, during which all surfactants and unreacted molecules were removed from the product. The resultant CB-PAA nanoparticles were freeze-dried and stored for later use.

2.2.4a Characterization

CB-PAA NPs were dissolved in DPBS, syringe filtered (Whatman, 0.2µm pore size) and diluted to 0.05 mg/mL, after which the size and zeta potential of nanoparticles were measured using a DelsaNano DLS particle sizer (Beckman

Coulter, Brea, CA). Representative sizing and zeta potential data is shown in Figure 2.1. The percent of Coomassie Blue dye in each batch of nanoparticles was calculated, based on a standard calibration curve of the dye's absorption at 597nm. Two batches of NPs were used; the NPs used in the MTT assays and PTT experiments had 8.5% Coomassie Blue dye loading and NPs used for cellular uptake experiments had 11% dye loading.

The degree of photobleaching of the CB-PAA NP during PTT was determined by first measuring the absorbance of varying concentrations (0.1, 0.6, & 1.0 mg/mL) of CB-PAA dissolved in DPBS using UV-VIS spectrometry and then illuminating the samples for 40 minutes. The absorbance was again measured immediately following illumination. The degree of photobleaching was quantified as the percent difference in absorbance at 600nm before and after illumination. The absorbance of the CB-PAA NPs decreased a maximum of 40% after 40 minutes of illumination for all of the concentrations as shown in Figure 2.2.

To investigate if CB dye degrades out of the nanoparticle matrix during illumination the following tests was completed: CB-PAA NPs were dissolved in DPBS, illuminated continuously for 40 minutes and then filtered using a Whatman syringe filter (0.02 μm pore size) before the absorbance spectra was measured. As demonstrated by the large difference in the absorbance peaks, very little of the CB is degraded from the nanoparticles during illumination (Figure 2.3). Furthermore, for higher CB-PAA NP concentrations, it is likely that the very small absorbance peak of the filtrate is due to a small amount of nanoparticles

that were able to pass through the filter. We estimate the leaching to be well below 1%.

Singlet oxygen production during illumination of the CB-PAA was measured to ensure that singlet oxygen production did not contribute to CB-PAA nanoparticle induced cell kill. 2mL of a CB-PAA NP solution with a concentration of 0.6 mg/mL was thoroughly mixed with 80 µL or a 100µM stock solution of ADPA dissolved in DPBS. The solution was placed in a cuvette and irradiated at 600nm using an ozone-free xenon-arc lamp (150@, Jobin Yvon Horiba, slit width 10nm) while being constantly stirred at a moderate speed to ensure uniform suspension and oxygen diffusion. ADPA was excited at 378nm and the fluorescence measured at different time points over 10 minutes. The calculated k value for the CB-PAA NPs was 5×10^{-5} s^{-1} (Figure 2.4). Considering photobleaching of the ADPA, this indicates that the singlet oxygen production of the CB-PAA NPs is at least an order of magnitude lower than that of the nanoparticles conjugated with Methylene blue (9.4×10^{-4} s^{-1}), Photofrin (14×10^{-4} s^{-1}), and HPPH (1.23×10^{-4} s^{-1}), which are all photosensitizers routinely used in our lab for PDT[5,7,28].

The temperature change due heating caused by the CB-PAA NP alone in solution was measured by dissolving the NPs in DPBS at different concentrations and then illuminating the solution 40 minutes in a small petri dish. The temperature of the solution was monitored the entire duration of the illumination using a thermocouple that was attached to the middle of the plate and was recorded every four minutes. The measurements were carried out inside of a

humidified incubator at 37°. Two conditions were tested, the first with the temperature of the nanoparticle solution was approximately room temperature and the second where the solution was very near 37° before illumination began. The change in the temperature of the nanoparticle solution (ΔT) during the illumination time is shown in Figure 2.5.

2.2.4c CB-PAA Nanoparticle Solution Calibration

A known amount of previously freeze dried CB-PAA were dissolved in fresh DPBS (14040) to make a stock solution. The stock solution was then used to make diluted concentrations of CB-PAA solutions between 0.01-0.35mg/mL in DPBS with total volume of 1.5 mL each. The absorbance of dilute nanoparticle solutions was measured using Shimadzu UV-1601 Spectrophotometer; a representative plot is shown in Figure 2.6. A calibration curve relating CB-PAA NP concentration to absorbance at 600nm was constructed and fit linearly. The CB-PAA stock solution was then filtered using a 0.2 μm Whatman syringe filter; a small sample was taken and diluted to a concentration between 0.01-0.35mg/mL and the absorbance measured. The linear calibration curve was then used to extract the new concentration of the filtered nanoparticles. Losses due to filtering ranged between 0 – 30% depending on the amount of time the nanoparticles had been stored.

2.2.4d Cytotoxicity of the CB-PAA Nanoparticles

Cytotoxicity of the CB-PAA nanoparticles was tested with a standard MTT cell viability assay examining metabolically activity; cells that had not been incubated with any nanoparticles were used as a control. Cells were plated on a 96-well plate with a cell density of 5000 cells/well and cultivated overnight. CB-PAA nanoparticles and growth media were added into the wells so as to achieve for each sample an overall concentration ranging between 0.1-1.2 mg/mL and then incubated with the cells for 24 hours. The cells were then carefully washed and 200 µL of clear growth media plus MTT reagent were added (20µL of 5mg/mL of the MTT reagent dissolved in the 180 µL of media without FBS). After 4 hours, 200 µL of DMSO was added into each well, so as to solubilize the formazan crystals produced from the MTT in viable cells. The 96 well plates were covered with aluminum foil and placed on a rocking shaker (Reliable Scientific, Inc) and allowed to gently mix overnight in the dark. Absorption at 550 nm was measured, for each well, with a Molecular Devices Spectramax Plus 384 plate reader. The results from 24 wells for each nanoparticle concentration were analyzed. Coomassie blue dye related toxicity was not investigated in this study as no measurable toxicity was found in any of the previous studies completed in our group[17-20] and CB has been successfully utilized in both laboratory and clinical studies at concentrations much higher (10 and 20 fold) than those used in the present study[21,22].

2.2.5 Cellular Uptake Assay

Cells were grown to at least 90% confluency, passaged, and replated with half the initial concentration of cells. The cells were then allowed to reattach and grow overnight. Varying amounts of CB-PAA NP stock solution was mixed with growth media to achieve concentrations ranging between 0.1-1.2 mg/mL of particles in a total of 3mL of solution. After 24 hours, the cells were washed twice with DPBS and the particle solutions + media was added to the cells. The cells were allowed to incubate with the nanoparticle + media solution for 24 hours, then again washed twice with DPBS to remove free nanoparticles, trypsinized, and centrifuged for 5 minutes at 900 RPM. Trypsin, media and DPBS were aspirated, then 1.5 mL DPBS was added to the cells. 300μL of lysing reagent (Thermo Scientific, M-PER Mammalian Protein Extraction Reagent) was then added to each. For reference, cells that had been allowed to grow for the same amount of time without CB-PAA NP, were counted and adjusted so that their concentrations matched those of the cells incubated with particles. After 24hrs, the absorbance at 600nm was measured for the cells with CB-PAA, i.e. the amount of absorbance from the CB-PAA in the cells was measured using UV-VIS spectrometry with lysed reference cells. The spectra were then analyzed using a least squares method; the NP concentration, C_{NP}, was extracted by fitting the absorption spectrum to the linear combination:

$$R \cdot SPC_{ref} + C_{NP} \cdot SPC_{NP} + Const$$

where SPC_{ref} is the absorption spectrum of the lysed cells without NPs and SPC_{NP} is the absorption spectrum of NP solution in DI water. R and C_{NP} are the fitting parameters. The absorbance of the CB-PAA *only* was extracted from the analysis and converted to the corresponding concentration in mg/mL and then divided by the number of cells to get the average CB-PAA per cell.

2.2.6 Photothermal Therapy & Live/Dead Assay

CB-PAA nanoparticles dissolved in DPBS were mixed thoroughly with fresh growth media, added to cells and then allowed to incubate for 24 hours. The cells were washed twice with DPBS to remove any nanoparticles remaining outside of the cells, and new clear growth media was added (DMEM 21063). 5μL of 1.5 mM of Propidium Iodide dissolved in DMSO and 1μL of 2 mM of Calcein AM dissolved in DMSO was added to the cells and allowed to incubate for at least 10 minutes. Baseline measurements for the PTT were performed on an Olympus IX71 inverted microscope (Olympus America Inc., Melville, NY) using a 20x objective. The cells were then placed under the light source, for 10, 20 or 40 minutes, inside an incubator at 37° C and then immediately imaged following the treatment. The cells were then placed back in the incubator and only taken out for imaging at thirty-minute intervals for another 3 hours. The images were analyzed using Image J software to determine the number of live or dead cells per image, with the presence of Calcein AM fluorescence, indicating a live cell, and propidium iodide fluorescence in the nucleus indicating a dead cell (Figure 2.7).

2.2.7 Controls

Blank PAA NP in cells: Dried, blank PAA NPs were resuspended in DPBS and syringed filtered with a 0.2μm Whatman filter. Cells were incubated with 1.2mg/mL of blank PAA NPs solution for 24 hours and then washed thoroughly to remove any nanoparticles remaining outside of the cells. The cells were then illuminated for 40 minutes using the light source, after which the degree of cell death was quantified with the live/dead cell assay.

No NPs in cells: In order to investigate possible cell death caused by heating due to the light source alone, cells that had not been incubated with any NPs were illuminated with the light source continuously for 40 minutes. The degree of cell death over time after illumination was quantified with the live/dead cell assay.

2.3 Results & Discussion

2.3.1 Cytotoxicity

Many hydrogels, including PAA, have been used extensively in vivo, with no major toxic effects[4,24]. Furthermore, they are very flexible in their molecular engineerability, i.e. they can be modified for controlled, fast or slow, biodegradation. Nanoparticles of this type can also be optimized towards fast or slow dye delivery. Oftentimes, the NPS are PEGylated for controlled circulation time, and can be easily surface derivatized with molecular targeting moieties, e.g.

peptides or aptamers, to achieve high specificity to certain cancer cells[4,23]. Radiolabled, pharmokinetic studies have been conducted on PAA NPs with, and without, the biodegradable crosslinker in the NP matrix. In the case of NPs without the biodegradable crosslinker, the NPs have "shown tissue distributions of the PAA nanoparticles in the reticular endothelial systems that are consistent with other nanoparticle studies"[4]. No adverse effects were found when NPs with the biodegradable crosslinkers were utilized up to 90 days post treatment[4,6,23,24].

As shown in Figure 2.8, there was no significant difference in cell viability among cells incubated for 24 hours with CB-PAA with concentrations ranging between 0.1 and 1.2 mg/mL and the control (no nanoparticles) indicating the absence of any measurable dark toxicity associated with the nanoparticles. We note that the nanoparticles stay inside the cells, and that the cancer cells used in the present study divide after approximately 24 hours (the normal cell division being another indicator of the non-toxicity of these NPs in the dark). We also note that in potential medical applications, the effectivity of the nanoparticles after long times is irrelevant because the patient would not have to wait much longer than 24 hours between administration of the NPs and the treatment. Furthermore, cytotoxicity due to dye leaching was not investigated in the present study because dye leaching of CB-PAA NPs was investigated and quantized in a previous study and published work completed in our group. The study was conducted under simulated physiological conditions and demonstrated that the "covalent linkage of the CB molecule to the NP matrix polymer backbone *completely eliminates* dye leaching."[19]

2.3.2 Cellular Uptake

As shown in Figure 2.9, the average amount of CB-PAA nanoparticles taken up by the cells increases with increasing NP concentration until 0.4mg/mL, after which the uptake of nanoparticles into the cells increases only moderately nearing saturation. These results are similar to findings from studies on the uptake of targeted gold and iron oxide hybrid nanoparticles11 and chitosan-coated silver nanoparticles by two colorectal cancer cells[13]. PAA NPs can be targeted with the addition of targeting peptides, usually F3 or TAT, via simple wet lab techniques. Multiple cell lines have been successfully targeted using PAA nanoparticles[5,17,20,25]. Specifically, the addition of targeting moieties to the CB-PAA has been shown to require shorter incubation times and result in preferential uptake in cancerous cells, versus non-targeted NP[17,18]. Thus, the targetability of the CB-PAA NPs would enable further optimization of this mode of PTT through the likely decrease in the required nanoparticle concentration necessary for inducing thermolysis. The present study was a proof of principle study completed in vitro, so cell specific targeting was unnecessary at this initial step.

2.3.3 Photothermal Therapy

Nanoparticle concentration effects: The survival rate (over time) of cells that had been incubated with CB-PAA NP ranging from 0.2-1.2 mg/mL, and illuminated for 20 minutes is depicted in Figure 2.10. Cells that had been incubated with CB-PAA concentrations of 0.2-0.8 mg/mL experienced little to no

cell death during treatment; however, cells treated with the highest concentration of CB-PAA exhibited a survival rate of only 70% when imaged immediately after treatment. Furthermore, 1.5 hours post-treatment, more than 90% cell death was observed for the cells incubated with 1.2 mg/mL of CB-PAA. Nearly complete cell death was also observed 3 hours post-treatment for cells incubated with 0.6 and 0.8 mg/mL of CB-PAA. Cells treated with 0.2 and 0.4 mg/mL experienced only 22 and 33% cell death, respectively, 3 hours post-treatment. Interestingly, increasing the CB-PAA concentration from 0.4 to 0.6 mg/mL resulted in the observation of a particularly dramatic 14-fold increase in cell death after 3 hours. As a control, cells were incubated with 1.2 mg/mL of bank polyacrylamide nanoparticles **without** dye and illuminated for 40 minutes. The efficacy of the photothermal therapy increases with increasing nanoparticle concentration despite the notably smaller increase of uptake CB-PAA after 0.4 mg/mL. This somewhat surprising result may suggest a threshold beyond which changes in intracellular nanoparticle distribution cause a more efficient local thermolysis although, on average, the overall nanoparticle uptake increases very slightly. This is under further study.

Illumination time effects: Cell viability as function of exposure time of cells that had been incubated with 0.6 mg/mL CB-PAA NP and illuminated for 10, 20, and 40 minutes, is shown in Figure 2.11. 10 minutes of PTT yielded a death rate of only about 20% of the cells at 3 hours post-treatment; however, when the irradiation time was doubled, the efficacy of the photothermal therapy increased dramatically, yielding a 95% cell death at 3 hours post-treatment. When the PTT

treatment time is increased even further to 40 minutes, only 35% of the cells survived the treatment and complete cell death is observed at one hour post-treatment. Control experiments, where cells incubated with 1.2 mg/mL of blank PAA NP for 24 hours and irradiated for 40 minutes exhibited only 5% in cell death 3 hours post-treatment. This suggests that the major impetus of thermolysis induced cell death is the intracellular heating due to the covalently linked CB-PAA and not local or external heating due to the light source or any scattering effects.

2.4 Conclusions

The present work is a proof of principle study, which establishes the feasibility of a third modality, photothermal therapy, of the CB-PAA NPs. These nanoparticles have been successfully used for both surgical delineation and photoacoustic imaging[17-20]. Although Poly(acrylamide) gel is not FDA approved for use in nanoparticle mediated PTT of cancer cells, it has been successfully utilized in *in vivo* and *in vitro* studies for many years. PAA has also been used successfully in implants in animal models[24,26]. The pharmacokinetics, biodistribution, bioelimination, and toxicity of PAA gel nanoparticles have been studied *in vivo* and no acute toxicity has been associated with potentially therapeutic doses[4,26-28].

In the present study, the covalently-linked Coomassie blue polyacrylamide nanoparticles have been shown to be very effective in causing PTT induced thermolysis in HeLa cells for varying nanoparticle concentrations and treatment

times. This study can be used as demonstration that after the CB NPs are used to delineate a tumor and the majority of it is surgically excised, any remaining cancerous tissues can be located and destroyed by exploiting the photoacoustic imaging and photothermal therapy modalities without a need for another NP administration. Note that during or right after surgical debulking, any wavelength light source can be easily directed at the tumor residues. *In vivo* studies will follow. For optimal future use in *in vivo* studies, the nontoxic CB-PAA NPs used in this study can be further optimized, to be targeted and biodegradable, as was demonstrated before with PAA NPs[4].

2.5 Acknowledgments

The authors would like to acknowledge Dr. Michael Nie, Matthew Waugh, and Lydia-Ann Ghuneim.

2.6 Figures

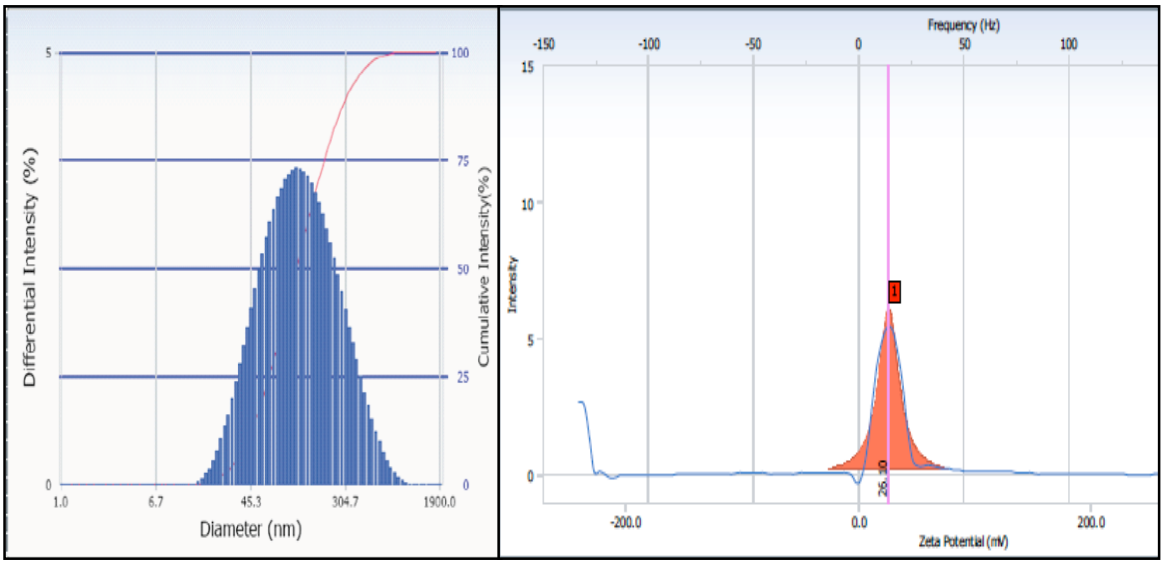

Figure 2.1: Size and zeta potential characterization of the CB-PAA NP was carried out using a Delsa Nano DLS particle sizer. CB-PAA NP are 80-95nm in diameter and have a zeta potential of 25-27mV.

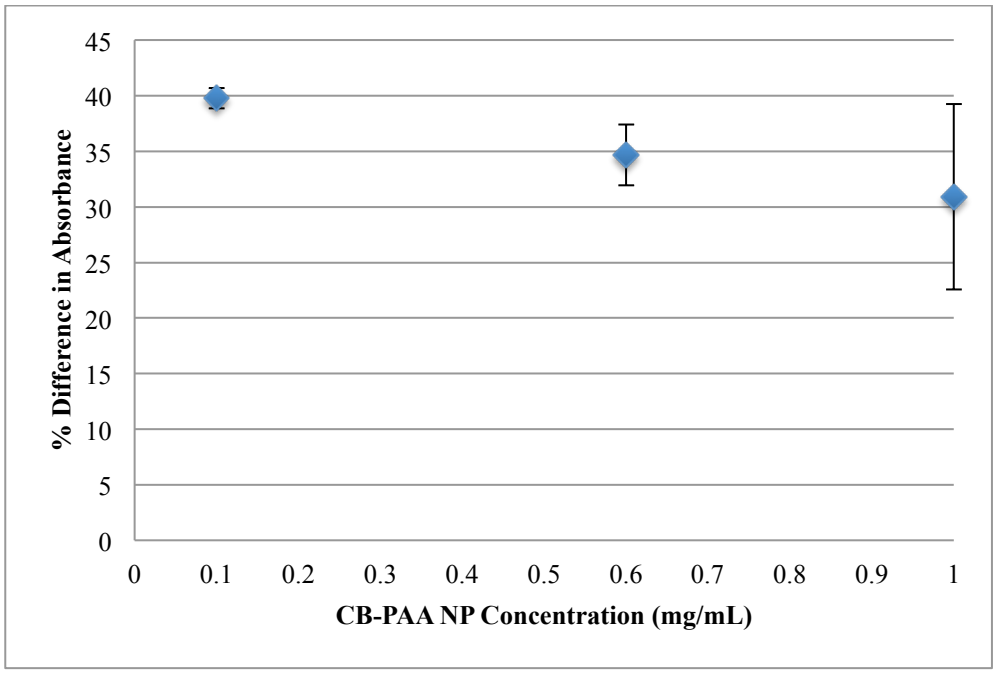

Figure 2.2: Photobleaching of various concentrations of CB-PAA nanoparticle solutions. The degree of photobleaching was quantified as the percent difference in absorbance at 600nm before and after illumination. Error bars denote standard error, n=2.

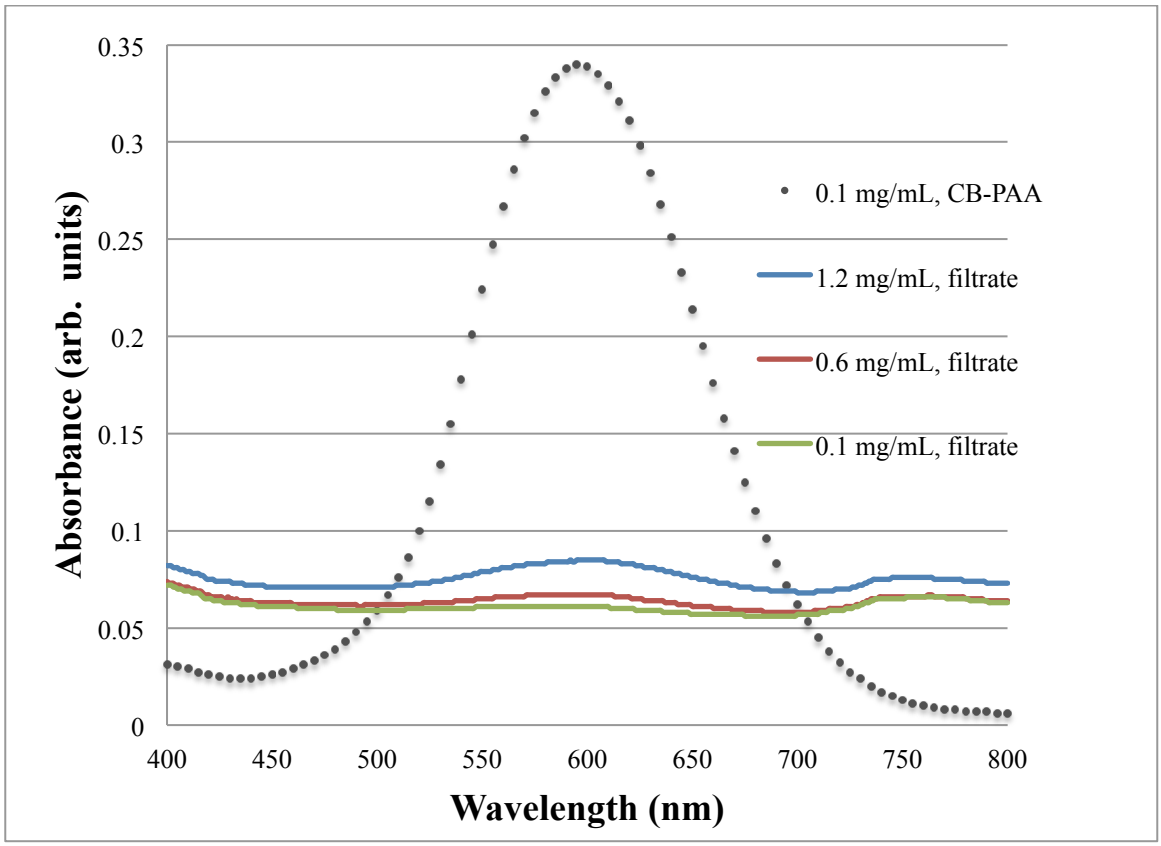

Figure 2.3: Absorbance spectra of the filtrate of varying concentrations of CB-PAA NP solutions *after* 40 minutes illumination. The absorbance spectrum of 0.1mg/mL of CB-PAA NPs is also displayed for reference.

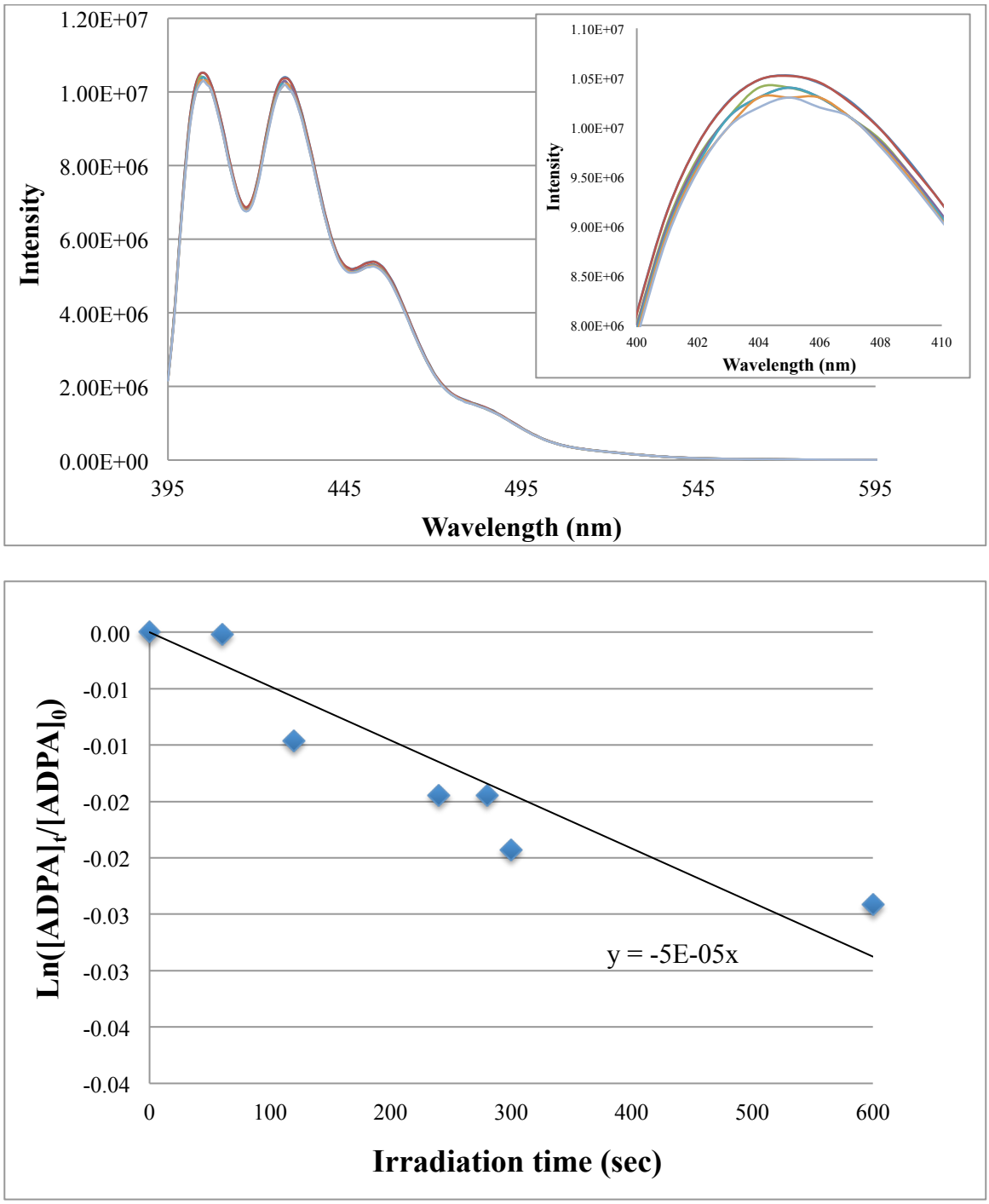

Figure 2.4: Top-Fluorescence spectra of ADPA in a mixed solution of CB-PAA NPs (0.6 mg/mL) at various time points; inset-close up view of 405nm peak used for calculations. Bottom-Linear fitted graph of fluorescence change with increasing irradiation times up to five minutes.

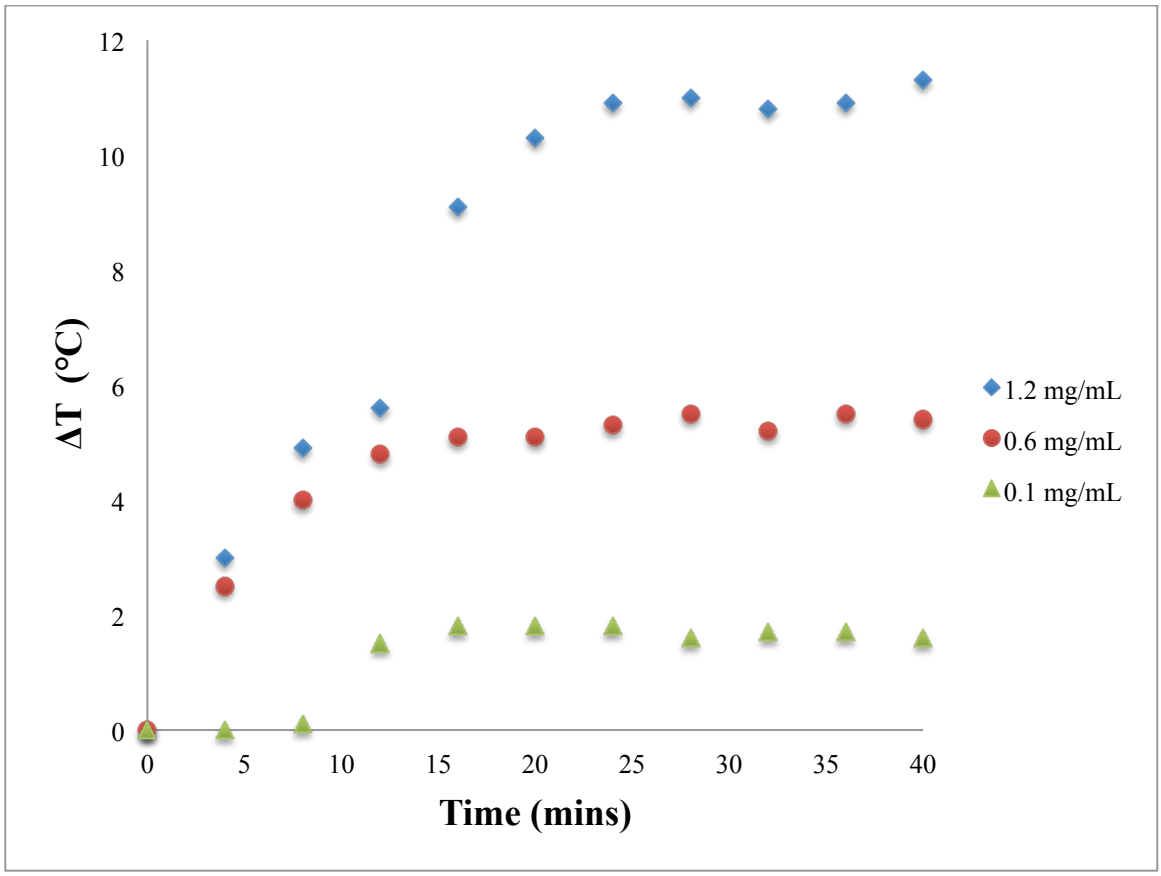

Figure 2.5: Temperature change for CB-PAA NP dissolved in DPBS at concentrations of 0.1, 0.6, and 1.2mg/mL. Initial starting temperature of the solutions was approximately 37° C.

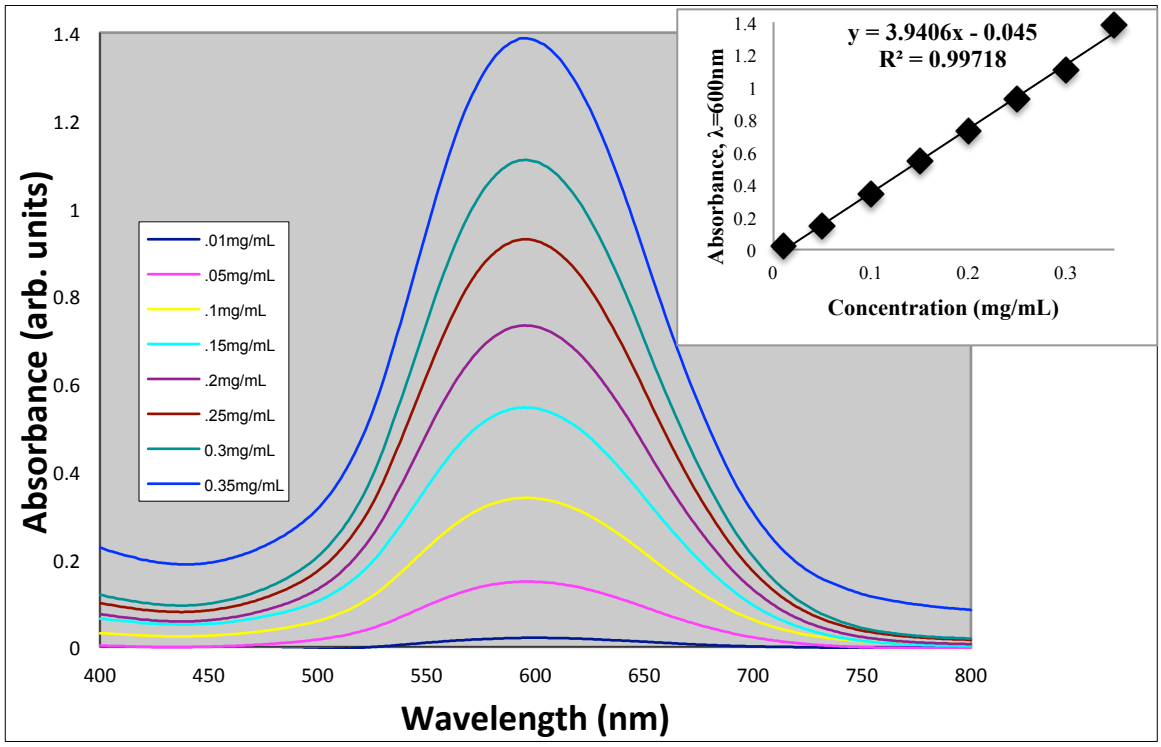

Figure 2.6: Absorbance of CB-PAA NP dissolved in DPBS at concentrations between 0.1-0.35mg/mL; inset: graph of CB-PAA NP concentration versus peak absorbance value at 600nm used to calculate the concentration of filtered CB-PAA NP.

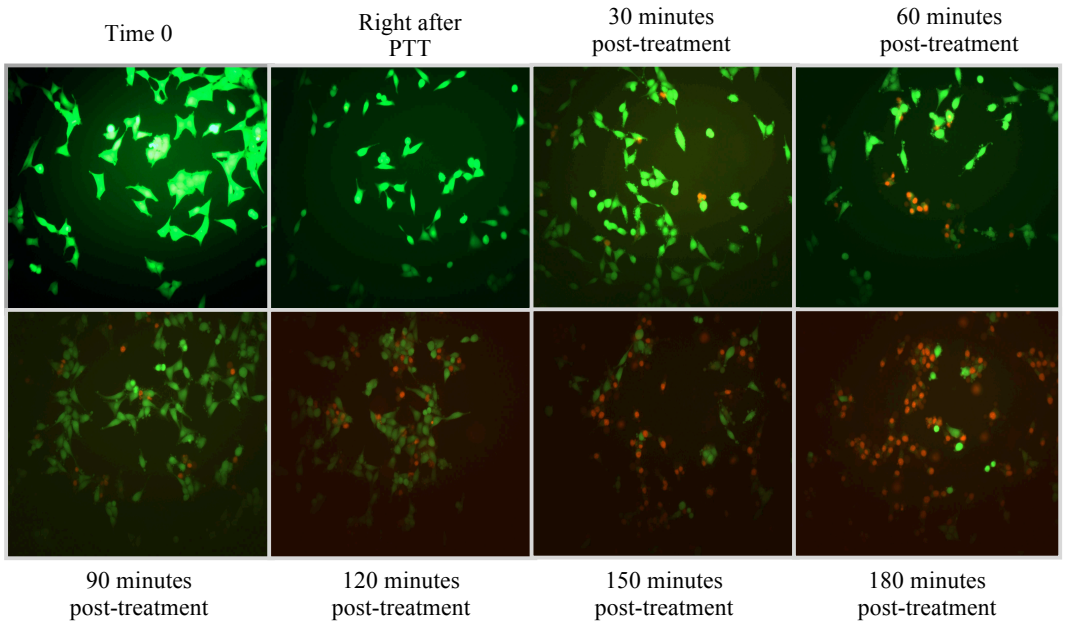

Figure 2.7: Fluorescent images of cells that had been previously incubated with CB-PAA NP and then exposed to PTT. The images were taken before, right after, and every 30 minutes post treatment. Green fluorescence indicates viable cells while red indicated dead cells.

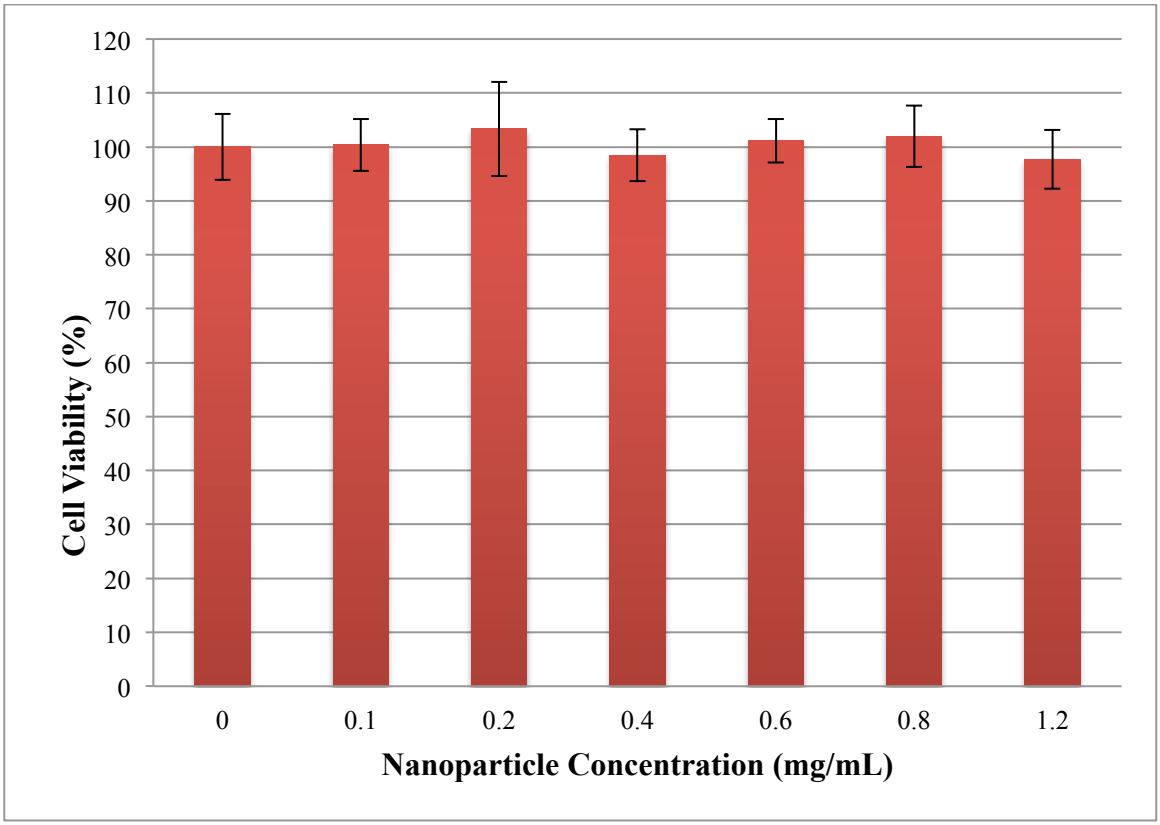

Figure 2.8: Cell viability of HeLa cells after 24 hours incubation with increasing concentrations of CB-PAA nanoparticle solutions as determined by MTT assay. The results indicate no significant change in toxicity with increasing nanoparticle concentration. Error bars represent standard error in absorbance at 550nm. Note: No illumination.

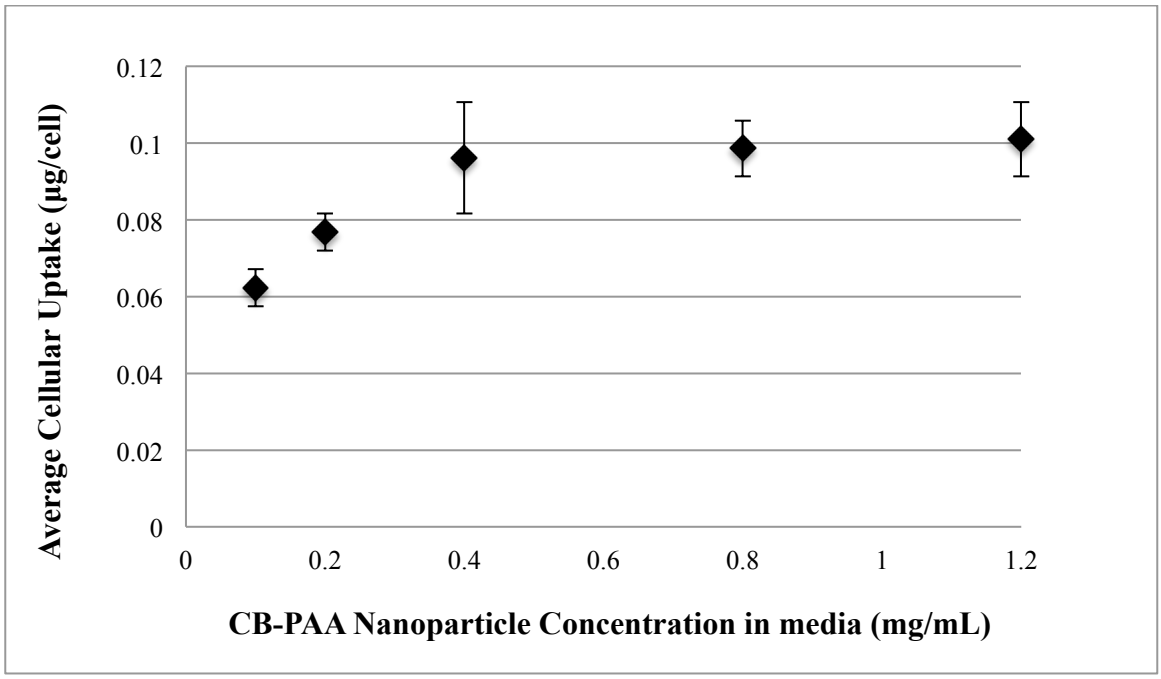

Figure 2.9: CB-PAA NP uptake into cells after 24 hours of incubation analyzed by nanoparticle absorbance at 600nm. Error bars denote standard error (n=2).

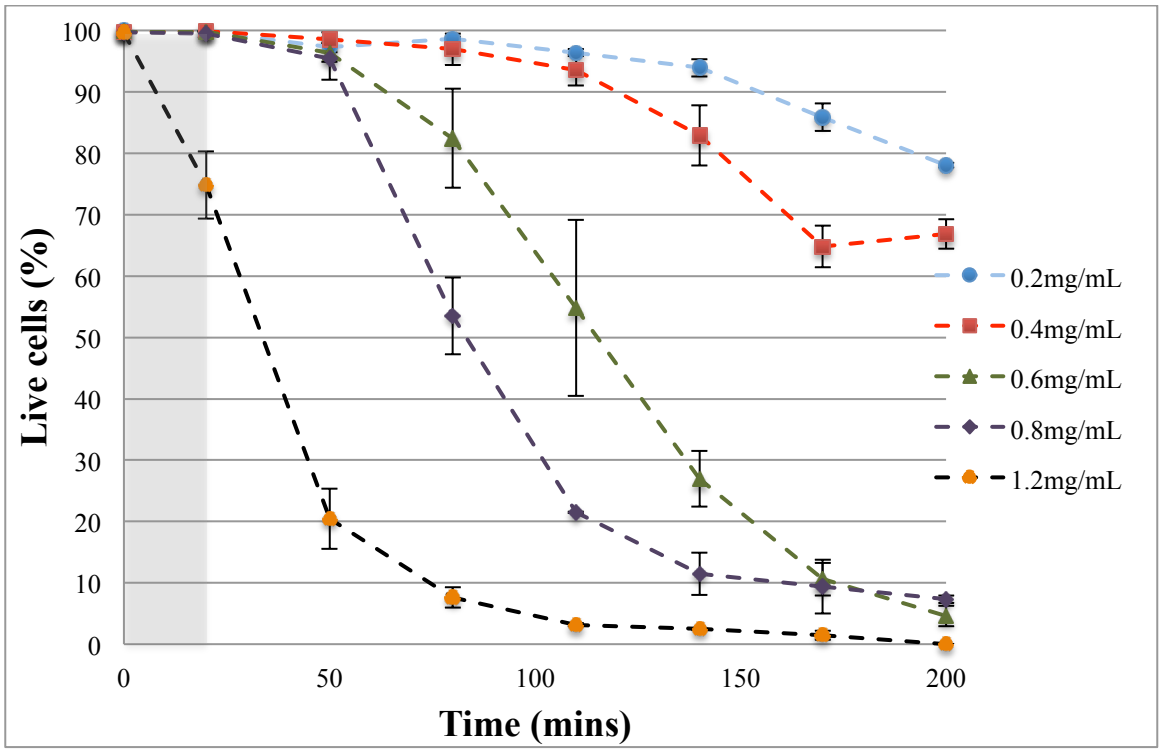

Figure 2.10: Survival rates over time of the cells over a period of 3 hours after 20 minutes of PTT with CB-PAA NP solution concentrations of 0.2-1.2mg/mL. Error bars denote standard error in average number of live cells per time point; experiments were done in triplicates, except for 0.8mg/mL, which was done in duplicate. Note: Shaded area is illumination time.

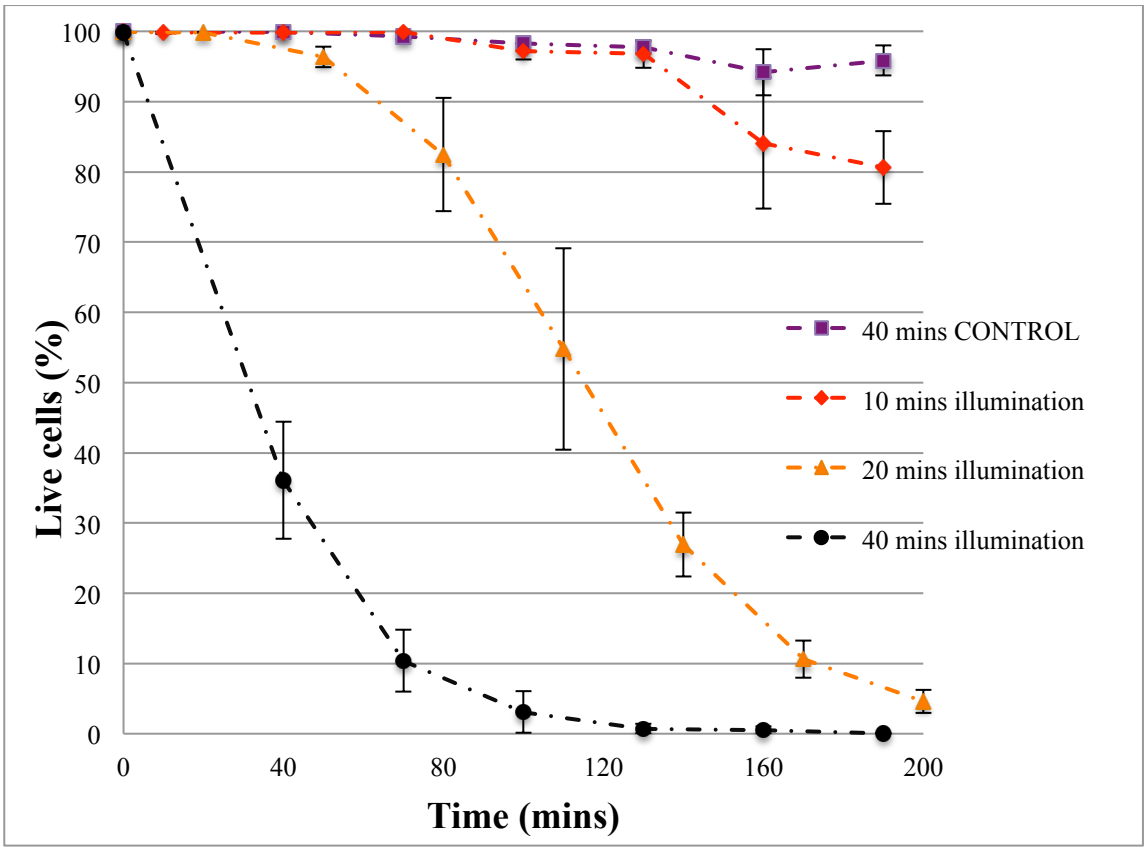

Figure 2.11: Survival rates over time of cells treated with 0.6 mg/mL of CB-PAA in growth media for 24 hours with 10, 20, and 40 minutes of illumination time (PTT), and the control measurement (BLANK PAA NP, 40 minutes illumination time). Error bars represent the standard error in the average number of live cells at each time point; experiments were done in triplicates. All illuminations started at time 0.

2.7 References

1. Siegel R, Ward E, Brawley O *et al*. Cancer statistics, 2011. *CA: A Cancer Journal for Clinicians*. 61, 212-236 **(2011)**.

2. Jain PK, Lee KS, El-Sayed IH *et al*. Calculated absorption and scattering properties of gold nanoparticles of different size, shape, and composition: applications in biological imaging and medicine. *J. Phys Chem. B.* 110, 7238-7248 **(2006).**

3. Kopelman R, Philbert M, Koo YEL *et al.* Multifunctional nanoparticle platforms for in vivo MRI enhancement and photodynamic therapy of a rat brain cancer. *J. of Magnetism and Magnetic Materials.* 293, 404-410 **(2005).**

4. Koo YEL, Reddy GR, Bhojani M *et al.* Brain cancer diagnosis and therapy with nanoplatforms. *Adv. Drug Deliv. Rev.* 58(14), 1556-1577 **(2006).**

5. Hah HJ, Kim G, Koo, YEL *et al.* Methylene blue-conjugated hydrogel nanoparticles and tumor-cell targeted photodynamic therapy. *Macromol. Biosci.* 11, 90-99 **(2011).**

6. Huang HC, Barua S, Sharma G *et al*. Inorganic nanoparticles for cancer imaging and therapy. *Journal of Controlled Release.* 155, 344-357 **(2011).**

7. Reddy GR, Bhojani M, McConville P *et al.* Vascular targeted nanoparticles for imaging and treatment of brain tumors. *Clin Cancer Res*. 12, 6677-6686 **(2006).**

8. Pan Y, Neuss S, Leifert A *et al.* Size-dependent cytotoxity of gold nanoparticles. *Small*. 3(11), 1941-1949 **(2007).**

9. Kobayshi, T. Cancer hyperthermia using magnetic nanoparticles. *Biotechnol. J.* 6, 1342-1347 **(2011).**

10. Bardhan R, Lal S, Joshi A *et al*. Theranostic nanoshells: from probe design to imaging and treatment of cancer. *Accounts of Chemical Research*. 44(11), 936-946 **(2011).**

11. Kirui DK, Rey DA, Batt CA. Gold hybrid nanoparticles for targeted phototherapy and cancer imaging. *Nanotechnology.* 21(10), 105105 **(2010).**

12. El-Sayed IH, Huang X, El-Sayed MA. Selective laser photo-thermal therapy of epithelial carcinoma using anti-EGFR antibody conjugated gold nanoparticles. *Cancer Letters.* 239, 129-135 **(2006).**

13. Boca SC, Potara M, Gabudean AM *et al*. Chitosan-coated triangular silver nanoparticles as a novel class of biocompatible, highly effective photothermal tranducers for in vitro cancel cell therapy. *Cancer Letters*. 311*,* 131-140 **(2011)**.

14. Alkilany AM, Nagaria PK, Hexel CR, *et al*. Cellular uptake and cytoxicity of gold nanorods: molecular origin of cytotoxity and surface effects. *Small.* 5(6), 701-708 **(2009).**

15. Chen YS, Hung YC, Liau I *et al*. Assessment of the in vivo toxicity of gold nanoparticles. *Nanoscale Res Lett.* 4, 858-864 **(2009)**.

16. Hrkach J, Von Hoff D, Ali MM *et al.* Preclinical development and clinical translation of a PSMA-targeted docetaxel nanoparticle with a differentiated pharmacological profile. *Sci. Transl. Med.* 4(128), *128ra39* **(2012).**

17. Orringer DA, Koo YEL, Chen T *et al. In vitro* characterization of a targeted, dye-loaded nanodevice for intraoperative tumor delineation. *Neurosurgery.* 64(5), 965-972 **(2009).**

18. Orringer DA, Chen T, Huang DL *et al.* The brain tumor widow model; a combined cranial window and implanted glioma model for evaluating intraoperative contrast agents. *Neurosurgery.* 66, 736-743 **(2010).**

19. Nie G, Hah HJ, Kim G *et al.* Hydrogel nanoparticles with covalently linked coomassie blue for brain tumor delineation visible to surgeon. *Small.* 8(6), 884-891 **(2012).**

20. Ray A, Wang X, Koo YEL *et al.* Targeted blue nanoparticles as photoacoustic contrast agent for brain tumor delineation. *Nano. Res.* 4(11), 1163-1173 **(2011)**.

21. Meyer C (ed). Vital Dyes in Vitreoretinal Surgery. *Dev Ophthalmol*. Basel, Karger, 42, 101-114 **(2008).**

22. Weng P, Cotrina M, Han X *et al*. Systematic administration of an antagonist of the ATP-sensitive receptor P2X7 improves recovery after spinal cord injury. *Proceedings of the National Academy of Sciences of the United States of America. 106* (30), 12489-12493 ***(*2009)**.

23. Grislain L, Couvreur P, Lenaerts V *et al*. Pharmacokinetcs and distribution of a biodegradable drug carrier, *Int. J. Pharm*. 15, 335-345 **(1983**).

24. Davis B. Diffusion in polymer gel implants.. *Proceedings of the National Academy of Sciences of the United States of America***.** *71* (8), 3120-3123 **(1974)**.

25. Lee YEK, Ulbrich E, Kim G *et al*. Near Infrared Luminescent Oxygen Nanosensors with Nanoparticle Matrix Tailored Sensitivity. *Analytical Chemistry. 82* (20), 8446-8455 **(2010).**

26. Lee YEK, Kopelman R. Targeted, Multifunctional Hydrogel Nanoparticles for Imaging and Treatment of Cancer. In: *Multifunctional Nanoparticles for Drug Delivery Applications: Imaging, Targeting, and Delivery,* Nanostructure Science and Technology. Svenson S & Prud'homme R (Eds.)*,* New York, USA 225-255 **(2012)**.

27. Wenger Y, Schneider R, Reddy G *et al*. Tissue distribution and pharmacokinetics of stable polyacrylamide nanoparticles following intravenous injection in the rat. *Toxicology and Applied Pharmacology. 251* (3), 181-190, **(2011).**

28. Wang S, Fan W, Kim G *et al*. Novel Methods to Incorporate Photosensitizers Into Nanocarriers for Cancer Treatment by Photodynamic Therapy. *Lasers in Surgery and Medicin. 43* (7), 686-695*, (***2011)**.